Engineering Structures 178 (2019) 70–87

Contents lists available at ScienceDirect

Engineering Structures

journal homepage: www.elsevier.com/locate/engstruct

Evaluation of force fluctuations induced by vertical seismic component on reinforced concrete precast structures

Marco Bovo*, Marco Savoia

DICAM, University of Bologna, Italy

ARTICLE INFO

Keywords:
Vertical ground motion
Precast building
Seismic assessment
Vertical record selection
Pulse-velocity effects

ABSTRACT

In many documented cases, reinforced concrete precast structures collapse during strong earthquakes was ascribed to the combination of horizontal and vertical ground motion components. In fact, the vertical component can increase significantly the axial compression in columns, with a reduction of the section ductility of the columns subject to bending induced by horizontal forces. The vertical components can have also detrimental effect at the beam – column connection level. Starting from these evidence, the effects of the vertical seismic component in reinforced concrete precast buildings are investigated here. In particular, the attention is devoted to the assessment of the fluctuations of the axial force in columns and vertical forces at the beam – column connection level. The paper reports the main outcomes of a series of nonlinear time-history analyses performed on 48 finite element models representative of the behaviour of existing precast structures with hinged connections and single or multi-bay, single or multi-storey, characterized by strong connection-weak column failure mechanisms. Far fault and near fault excitation types have been considered. Pulse-type velocity records were further considered in order to identify if they can cause possible amplification of seismic effects. Numerical outcomes are reported in terms of force response of a synthetic parameter α, ratio between vertical force induced by ground motion and that due to gravitational load. For this ratio, an analytical expression is proposed and calibrated based on numerical results. The proposed analytical relation, valid for the class of studied buildings, can be considered for design purpose as a more reliable alternative to the response spectra analysis with the current version of design vertical spectra of the Eurocode to assess the vertical force fluctuations on columns and connections. Lastly, different seismic intensity measures are considered in order to define the best predictor of the seismic vertical force fluctuations expected for this class of buildings.

1. Introduction

Nowadays, is well established that the vertical seismic component could play a significant role in the seismic damaging phenomena of reinforced concrete (RC) structures, also modifying the failure mode of a building [1–4]. Nevertheless, only recently the vertical component of the seismic action was considered in the purpose design of new structures or in the seismic assessment of existing ones [5,6]. Due to the usual higher energy content of the seismic horizontal records, if compared with vertical motions, researchers attributed the major damaging potential to the effects of horizontal components. Consistently, most of the building codes prescribe to consider the vertical excitation only in very limited cases, with the possibility of neglecting it in ordinary design [7–10]. Moreover, due to the lack of deepened knowledge on vertical waves propagation and uncertainties in the attenuation laws [11–16], most of the international codes provide the Vertical Peak Ground Acceleration (PGA_V) as a percentage of Horizontal Peak Ground Acceleration (PGA_H) [17]. Nevertheless, some post-earthquake studies indicate that vertical excitation can be important especially for large span RC structures.

For instance, Kunnath et al. [18], although with specific reference to highway overcrossings, proved and quantified a significant increase of axial loads in bridge columns if compared to gravitational loads as the effect of the vertical components of near-fault records. Moreover, for those structures, they claimed that vertical effects may be uncoupled from horizontal effects and addressed the need for a distinct vertical spectrum for design.

With reference to buildings, the recent 2012 Emilia sequence, striking a wide area of Italian territory [19–25], as other notorious past earthquakes [26–31], highlighted the high vulnerability of RC precast structures not designed for seismic actions. In-field inspections on precast buildings with hinged connections (i.e., in the presence of

* Corresponding author.
E-mail addresses: marco.bovo@unibo.it (M. Bovo), marco.savoia@unibo.it (M. Savoia).

https://doi.org/10.1016/j.engstruct.2018.10.018
Received 28 March 2018; Received in revised form 13 August 2018; Accepted 8 October 2018
Available online 15 October 2018
0141-0296/ © 2018 The Authors. Published by Elsevier Ltd. This is an open access article under the CC BY-NC-ND license (http://creativecommons.org/licenses/BY-NC-ND/4.0/).

mechanical devices), revealed that some collapse modes were magnified by the presence of the vertical excitation component [32–35], the latter causing a modification of both demand and capacity of columns for horizontal action [36–40]. RC precast structures with friction-based supports (i.e. without mechanical connection devices) were even more sensitive to vertical action because of the additional failure modes due to the slipping between the precast elements at beam-column and floor slab-beam level due to the reduction of the resisting friction force.

These incontrovertible evidence, together with the scarcity of studies on this issue, encouraged researchers' work on the investigation of the effects of vertical motion on both precast and cast in-situ structures [6,41–43].

Recently, Magliulo et al. [44] performed the seismic assessment of existing precast structures with three different methods: elastic, nonlinear static and nonlinear dynamic analyses. The study examined two different structure typologies, concluding that the complex behaviour of the structure subject to the three components of the motion could be achieved only by a three-dimensional model and time-history procedure. Furthermore, the paper highlighted the limitations of simplified analyses even if the selected buildings were regular both in-plane and elevation.

Liberatore et al. [33] found that, if the seismic vertical component is neglected or taken into account, the failure scenario of precast structures can be completely different, with the formation of plastic hinges at the base of the columns on one hand and activation of sliding movements between precast elements on the other. Furthermore, ground motions with different PGV_V/PGA_V ratios (i.e. Vertical Peak Ground Velocity / Vertical Peak Ground Acceleration) were considered.

Casotto et al. [45] generated seismic fragility curves of RC precast structures not designed against seismic actions considering the effects of vertical ground motion. Important findings evidenced that failure due to the slip at the supports, one of the most important collapse modes in no-seismically designed precast structures with friction-based connections, is correctly captured only performing inelastic time-history analyses with all the three ground motion components.

Belleri et al. [36] concluded that, neglecting the vertical ground motion, the safety factor related to sliding phenomena between precast elements could be overestimated of about 10%.

Furthermore, when simplified analyses are introduced in time-consuming seismic procedures to limit the computational effort, the effects of the vertical seismic action are introduced in the models in approximately way on the base of engineering judgement or experience [45,46]. Typically, a reduction coefficient is applied on the static vertical load due to self-weight of structural and non-structural elements, but without considering the real dynamic vibrating properties of buildings in the vertical direction. This could bring to considerable uncertainties on the outcomes if the coefficient is not properly established.

The role of connection devices in precast structures have been also the subject of many experimental researches on full-scale or scaled RC precast structure samples, in order to define the main features of this building class. In [47], the seismic response of two 3:4-scale two-bay, three-story precast concrete frames with and without cladding panels was examined in an experimental program considering a quasi-static cyclic displacement history. In [48], a full-scale three-storey precast building was subjected to a series of pseudo-dynamic tests. The experimental campaign considered four different structural configurations: shear walls and hinged beam-column joints, hinged beam-column joints, hinged beam-column joints at the first and second floor and moment-resisting at the third, moment-resisting beam-column joints. The experimental outcomes indicated that the seismic response of the various systems greatly depends on the behaviour of the connection system, and the key role played by proper design and detailing of the joints, all this influencing both the kinematics of the system and the damaging mechanism.

In fact, as experimental test revealed [49,50], the presence of mechanical devices between precast elements (typically dowels in beam-column connections and steel plates in floor slab-beam connections) increases in a considerable way the capacity of the connections with respect to friction-based support, and could activate the formation of the plastic hinge at the base of the column.

Starting from these emerging outcomes, the effects of the seismic vertical component on RC precast structures are investigated in the present paper by means of time-history analyses on a wide stock of three-dimensional single or multi-bay, single or multi-storey, inelastic models of existing buildings. The paper refers in particular to precast structures with hinged storey elements with strong connection-weak column failure mechanism. Despite the large number and different typologies of precast structures considered, the structural models considered in this study can be representative of a wide number of existing structures for this particular class of buildings.

In particular, the attention is devoted to the estimate of the fluctuations of axial column forces and vertical forces at the supports of precast elements. An approximate expression, providing the maximum (i.e. peak) variation of axial force in columns and vertical force on connections starting from the value of vertical vibration period of structure and PGA_V, is introduced and described in the paper. It can be seen as a force response spectra available for the first vertical period range of the building stock (i.e. 0.025–0.5 s). The relation is calibrated with reference to both far fault and near fault earthquake records. For design purposes, the present analytical expression gives estimates of vertical fluctuation more reliable than those obtained by response spectra analyses, which systematically underestimate those obtained by time-histories. Finally, a case study, where the proposed expression is tested and validated, is presented.

2. Ground motion selection

In the present study, a first ground motion database of 751 vertical acceleration records was selected to cover a wide range of frequency content, time duration and amplitude, with reference to the vertical seismic component. The records, extracted from Pacific Earthquake Engineering Research Center (PEER) strong motion database [51], were selected in the range of moment magnitude Mw from 4.0 to 7.9, with a PGA_V ranging from 0.1*g* to 1.0*g*, a distance from causing source between 0 km and 200 km, A, B or C site classes according to Eurocode 8 (EC8) [9], and considering only vertical records that do not present pulse-velocity shape according to the criteria given in [52]. Fig. 1 reports the distribution of the records in terms of *Mw* and distance.

The records were classified into two groups, i.e. near fault (NF) without pulse-velocity shape and far fault (FF) excitations, in order to perform comparisons of the building response for different excitation types [53]. It is worth noting that the usual criteria adopted to select

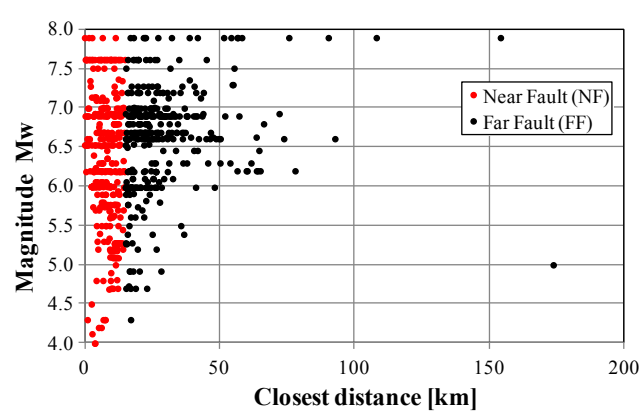

Fig. 1. 397 Near Fault without pulse-velocity shape (NF) and 354 Far Fault (FF) vertical ground motion records selected for time-history analyses: distribution in terms of moment magnitude *Mw* and closest distance to causing source.

and scale records for seismic analyses are typically referred to the horizontal components of the acceleration, and the distinction between near fault and far fault excitations is usually done with reference to those components. Identification criteria proposed by various authors (e.g. [54–57]) are then not appropriate for the purpose of the present study. Then, in this work, the criterion adopted to distinguish NF from FF ground motions is based on their distance from the causing seismic source and, as proposed in [13], a distance of 15 km was adopted as the threshold value. In the absence of information about the fault distance, the epicentre distance was considered. Both NF and FF groups, including 397 and 354 records respectively, were divided into subsets with increasing levels of PGA_V. Five record subsets were defined for the NF group (0.1–0.2*g*; 0.2–0.4*g*; 0.4–0.6*g*; 0.6–0.8*g*; 0.8–1.0*g*) with 189, 127, 48, 20 and 13 ground motions attributed to the various subset, respectively. For the FF group, records were grouped in four subsets (0.1–0.2*g*; 0.2–0.4*g*; 0.4–0.6*g*; 0.8–1.0*g*) with 270, 79, 3 and 2 ground motions (no FF records were found in the interval 0.6–0.8*g*). It is worth noting that the number of ground motions records in the last two subsets results rather poor to provide a meaningful statistical elaboration. Nevertheless, the outcomes of the two subsets have been maintained in order to provide a comparison with other subsets. No scaling of the records was adopted in the present work except for the study reported in Section 6. In Fig. 2a and b, the average elastic vertical spectra of each subset are reported, respectively, for NF and FF ground motions. Only for a general comparison, the elastic vertical spectra prescribed by EC8 are reported in the figure. They were obtained setting the values of PGA_V equal to the average PGA_V of each subset. As an important preliminary observation, is worth noting that EC8 elastic spectra present values of vertical acceleration systematically higher than those obtained from NF records. For FF, in subsets with very few records (0.4–0.6*g* and 0.8–1.0*g*) the values of vertical acceleration may overcome the EC8 spectra ordinates for some ranges of periods, but this is maybe to attribute to the poor number of ground motions available.

A further database of 40 near fault vertical ground motion records with pulse-velocity shape according to the criteria given in [52], were selected from the PEER strong motion database [51] for a comparison of the effects produced on precast structures respect to non-pulse-velocity accelerograms. The criteria reported in [58,59] were also checked to confirm the pulse-like ground motion features of the selected records. The pulse-velocity (PV) records were selected in the range of moment magnitude Mw from 4.0 to 7.9, with a PGA_V ranging from 0.1*g* to 1.0*g*, a distance from causing source between 0 km and 15 km, A, B or C site classes according to EC8, for strike-slip, normal, reverse or reverse oblique, faults considering a pulse period T_p smaller than 15 s, and for *PGVv* between 5 cm/s and 250 cm/s. The PV database was then divided into three subsets (characterized by different PGA_V values), in order to compare results with those obtained by NF motions (without pulse-velocity shape) for analogous levels of vertical acceleration. The three subsets, with PGA_V in the intervals 0.1–0.2*g*, 0.2–0.4*g* and 0.4–0.6*g*, contained respectively 10, 18 and 12 PV ground motions. The main characteristics of PV motion database are summarized in Table 1. Elastic spectra of PV records are not reported because, as well known, they are not representative of the dynamic behaviour of the structures under a pulse-type motion. In the following, we will show as pulse-velocity vertical records produce seismic forces in precast structures higher than non-pulse-velocity ground motions.

3. Building stock definition

3.1. Typology and geometry of the selected buildings

A stock of 20 existing RC precast structures (labelled S1–S20) was considered in the study. The buildings were built between 1968 and 2005. Some of them have been designed against seismic actions by following the design rules of the construction age. In any case, no one matches the actual seismic prescriptions by following actual Italian Building Code [10] or EC8 [9]. In the stock, 15 buildings were single-storey, 2 buildings were two-storey and 3 were three-storey buildings. Four additional structures (virtual structures defined as V1–V4) were added to complete the stock by varying some geometrical properties of structure S11, as described in the following. The structures considered in the study, typical of most of the European technologies for precast buildings, have columns clamped at the base and hinged horizontal beams and floor slab elements with the presence of mechanical devices (steel dowels or steel plates). Data on geometry, materials, dead and live loads for the structures were obtained from as-built projects; the main structural parameters of each building are reported in Table 2. The main information on dimensions, materials, reinforcement bars (rebars) of vertical elements is collected in Table 3. The material class applies also to horizontal elements of the building. The selected building stock includes seven typologies of precast main beams and six types of precast slab elements constituting the storey/roof levels. Main beams have span ranging from 6 m to 30 m while, for the slab elements, between 7 m and 28 m. The height of the single-storey buildings ranges from 5 m to 9 m. For the multi-storey structures, the interstorey height ranges from 3 m to 8 m. Columns have rectangular or squared cross-section. The self-weight of structural elements is calculated starting from the sizes of precast elements. The additional distributed gravity load (non-structural and live load) Q_{DL}, adopted to define the seismic combination according to EC8, was obtained for each building from its design documentation, and it ranges from 0.0 kPa to 5.0 kPa.

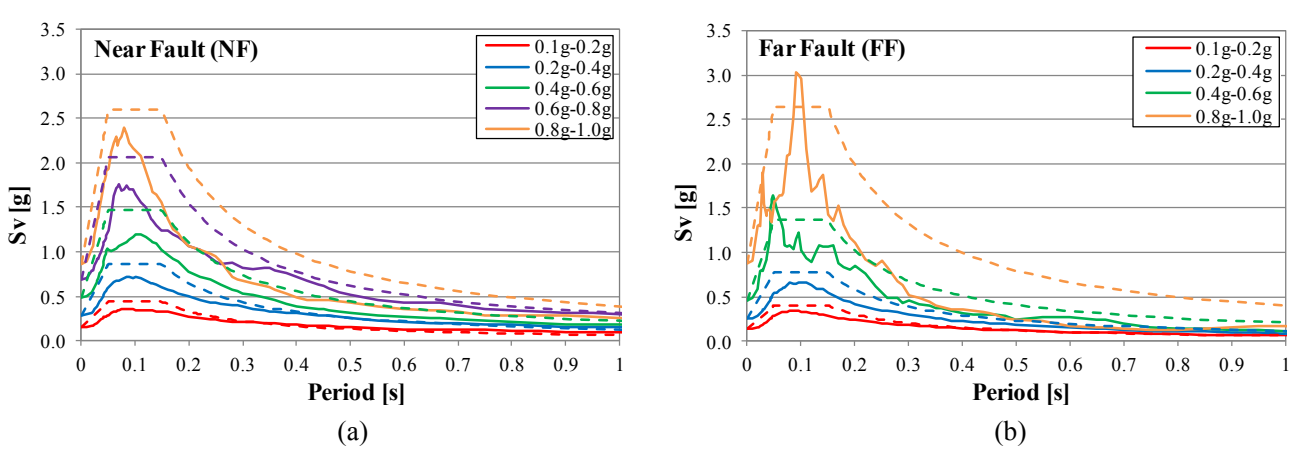

Fig. 2. Average acceleration response spectra of selected ground motions and comparison with the elastic spectra prescribed by EC8 for analogous values of PGA_V: (a) Near Fault (NF) subsets; (b) Far Fault (FF) subsets.

Table 1
Main parameters of the 40 near fault pulse-velocity ground motions (with SS: strike-slip faults; N: normal faults; R: reverse faults; RO: reverse oblique faults; *Tp*: pulse period; *Mw*: moment magnitude; *D*: closest distance between record station and causing seismic source; PGA_V, PGV_V, PGD_V: vertical peak acceleration, velocity and displacement).

Record number	Station name	Earthquake	Year	Fault type	*Tp* [s]	*Mw*	*D* [km]	PGA_V [g]	PGV_V [cm/s]	PGD_V [cm]
1	Gilroy Array #2	Coyote Lake	1979	SS	1.463	5.74	8.47	0.168	6.846	1.134
2	Gilroy Array #4	Coyote Lake	1979	SS	1.351	5.74	4.79	0.422	15.279	2.777
3	Brawley Airport	Imperial Valley 06	1979	SS	4.396	6.53	8.54	0.153	8.739	3.604
4	El Centro Array #4	Imperial Valley 06	1979	SS	4.788	6.53	4.9	0.292	16.855	11.511
5	El Centro Array #5	Imperial Valley 06	1979	SS	4.13	6.53	1.76	0.594	39.515	22.324
6	Bagnoli Irpinio	Irpinia-Italy 01	1980	N	1.713	6.90	8.14	0.107	15.843	8.244
7	Sturno (STN)	Irpinia-Italy 01	1980	N	3.272	6.90	6.78	0.235	24.006	10.485
8	Coyote Lake Dam S.W.A	Morgan Hill	1984	SS	1.071	6.19	0.18	0.387	15.594	2.254
9	Gilroy Array #6	Morgan Hill	1984	SS	1.232	6.19	9.85	0.406	14.168	1.603
10	Nat. Geo. Inst.	San Salvador	1986	SS	1.127	5.80	3.71	0.460	19.154	2.518
11	Gilroy – Hist. Bldg.	Loma Prieta	1989	RO	1.638	6.93	10.27	0.148	12.559	8.319
12	Saratoga-Aloha Ave	Loma Prieta	1989	RO	4.571	6.93	7.58	0.396	27.991	17.268
13	Petrolia	Cape Mendocino	1992	R	2.996	7.01	0.10	0.165	20.354	20.195
14	Newhall – Fire St.	Northridge 01	1994	R	1.372	6.69	3.16	0.548	30.955	13.920
15	Pacoima Dam (downstr)	Northridge 01	1994	R	0.588	6.69	4.92	0.191	14.184	1.388
16	Pardee – SCE	Northridge 01	1994	R	1.232	6.69	5.54	0.385	11.106	0.485
17	KJMA	Kobe-Japan	1995	SS	1.092	6.90	0.94	0.339	40.354	14.434
18	Port Island (0 m)	Kobe-Japan	1995	SS	2.828	6.90	3.31	0.567	62.077	27.819
19	Gebze	Kocaeli-Turkey	1999	SS	5.992	7.51	7.57	0.194	14.114	5.774
20	Yarimca	Kocaeli-Turkey	1999	SS	4.949	7.51	1.38	0.242	30.763	29.543
21	TCU052	Chi Chi-Taiwan	1999	RO	11.956	7.62	0.11	0.197	143.981	154.050
22	TCU068	Chi Chi-Taiwan	1999	RO	12.285	7.62	0.15	0.530	213.013	222.680
23	TAPS Pump St. #10	Denali-Alaska	2002	SS	3.157	7.90	0.18	0.238	51.074	19.754
24	CHY074	Chi Chi-Taiwan 04	1999	SS	2.436	6.20	6.02	0.297	16.662	5.273
25	TCU078	Chi Chi-Taiwan 06	1999	R	4.151	6.30	5.72	0.312	21.754	14.403
26	TCU080	Chi Chi-Taiwan 06	1999	R	1.022	6.30	0.22	0.480	12.078	4.279
27	TTR008	Tottori-Japan	2000	SS	1.540	6.61	6.86	0.316	9.730	4.743
28	Parkfield – EADES	Parkfield 02-CA	2004	SS	1.218	6.00	1.37	0.196	7.370	1.377
29	Parkfield – Stone Corral 1E	Parkfield 02-CA	2004	SS	0.574	6.00	2.85	0.331	16.318	1.331
30	NIG021	Niigata-Japan	2004	R	0.322	6.63	10.21	0.573	13.192	3.752
31	NIGH11	Niigata-Japan	2004	R	1.799	6.63	6.27	0.320	12.668	6.227
32	Bar-Skupstina	Montenegro	1979	R	1.442	7.10	0.54	0.244	14.178	3.306
33	Hotel Olimpic	Montenegro	1979	R	1.974	7.10	3.97	0.461	15.155	6.610
34	L'Aquila – Centro Valle	L'Aquila-Italy	2009	N	1.071	6.30	0.32	0.529	12.400	3.134
35	L'Aquila – Parking	L'Aquila-Italy	2009	N	1.981	6.30	0.27	0.371	19.735	4.579
36	Joetsu Kakizakiku	Chuetsu Oki-Japan	2007	R	1.4	6.80	9.43	0.180	18.606	7.856
37	DSLC	Darfield	2010	SS	7.826	7.00	5.28	0.317	14.574	9.497
38	Resthaven	Christchurch-	2011	RO	1.554	6.20	5.11	0.522	20.989	7.423
39	El Centro Array #12	El Mayor Cucapah	2010	SS	8.722	7.20	9.98	0.275	17.030	9.250
40	IRIGM 487	Duzce-Turkey	1999	SS	10.052	7.14	2.65	0.229	14.719	14.168

3.2. Structural modelling

For each structure, two different three-dimensional finite element (FE) models were adopted for the study of the seismic behaviour when subject to vertical ground motion. In the first model, one bay of the structures was considered (*sb*: single-bay model) whereas, in the second one, two bays for both horizontal directions were modelled (*mb*: multi-bay model). Fig. 3 shows the FE models adopted in the present work. The columns were fully restrained at the base.

Modelling and structural analyses were performed with the software OpenSEES [60]. As far as the material constitutive models are concerned, Mander model [61] for concrete and Menegotto-Pinto model [62] for steel were adopted, assuming mean values for material properties. Mean values were defined for concrete according to Eurocode 2 (EC2) [63] and for the reinforcement steel from the database Styl [64], depending on the year of construction and the material classes reported in Table 4 as resulting from the design documentation of each building. The 1D finite elements, adopted for columns, beams and floor slab elements, have a flexibility formulation with a classical fibre subdivision over the cross-section and distributed plasticity [65]. The various interstorey/roof slab elements have been modelled with beam elements without introducing connections between them because of the lack, in the investigated buildings, of a structural RC topping or slab able to connect in a reliable way the elements along their lateral sides.

Connections between beam-column elements and roof slab-beam elements were modelled as depicted in Fig. 4. A horizontal rigid link has been inserted at the top of the column in order to introduce in the FE model the actual eccentricity of the beam support with respect to the vertical axis of the column. A zero-length element was then added between the two extremity nodes, connecting the translational DOFs without transmission of bending moment. In the horizontal directions (*x*- and *y*-axis in the reference system of Fig. 4), a rigid behaviour was assumed. In the vertical direction (*z*-axis in Fig. 4), a nonlinear law for the support connection was introduced with different behaviour in tension and compression. The connection is rigid in compression (i.e. when the gravitational load is greater than the seismic vertical seismic force), whereas it has an elastic-plastic behaviour under tension up to the plastic capacity of the mechanical devices (i.e. steel dowels). The axial stiffness in tension is $K_T = Es{\cdot}As/Ls$ (where *Es*: Young modulus of steel; *As*: cross-section of dowel and *Ls:* free length of dowels). Typically, the value of K_T is very high. In the applications presented, the plastic capacity (F_y) was never reached during time-history analyses.

The vertical natural period of the 40 buildings ranges from 0.13 s to 0.52 s. In order to assure a whole covering of the acceleration spectrum also in the very stiff building range (i.e. vertical period lower than 0.15 s), four additional virtual (V) buildings were defined by increasing the moment of inertia of beams and floor slab elements of the structure S11 (the one with the lowest vertical period in the stock – T_1 = 0.128 s). Taking the typical cross-section of beams and roof slab elements of structure S11 as the reference (see Fig. 4b), the section

Table 2
Precast buildings: main data on geometry and vertical loading collected from as-built projects (L_{beam} = span of the beams; S_{slab} = spacing of the floor slab elements; L_{slab} = span of the floor slab elements; H_{storey} = height of the building for one-storey buildings or height of the storey for multi-storey buildings; Q_{DL}: distributed static gravitational load in seismic combination excluding self-weight of the structural elements; (1): first floor in a multi-storey building; (2): second floor in a multi-storey building; (R): roof floor in a multi-storey building).

Structure	Beam typology	L_{beam} [m]	Floor slab typology	S_{slab} [m]	L_{slab} [m]	H_{storey} [m]	Q_{DL} [kPa]
S1	I-double tapered	15.8	Triple tee	2.5	10.0	5.0	0.50
S2	I-double tapered	27.0	Double tee	2.4	12.5	9.0	0.25
S3	I-double tapered	30.0	Triple tee	2.5	7.0	8.0	0.0
S4	Inverted tee	9.4	Double tee	2.5	15.4	6.0	0.0
S5	H-shaped	12.5	Y-shaped	5.0	20.0	5.0	0.50
S6	H-shaped	8.0	Y-shaped	3.0	20.0	6.0	0.50
S7	I-shaped	10.0	Y-shaped	5.0	28.0	8.5	0.30
S8	I-shaped	10.5	Y-shaped	5.0	26.0	7.5	0.20
S9	AASHTO	14.0	Rectangular box	2.8	16.0	7.0	0.30
S10	Channel	15.0	Rectangular box	4.5	14.0	7.5	0.50
S11	Channel	17.0	Rectangular box	3.2	10.0	5.5	0.50
S12	Inverted tee	10.0	Double tee	2.5	9.0	7.0	0.30
S13	Channel	16.0	Y-shaped	5.0	16.0	6.5	0.50
S14	Channel	16.0	Y-shaped	5.6	16.0	8.0	0.50
S15	H-shaped	12.0	Y-shaped	3.2	18.0	5.5	2.50
S16(1)	Inverted tee	6.0	Double tee	2.5	7.5	3.80	5.0
S16(R)	I-double tapered	15.0	Double tee	2.5	12.0	3.80	0.2
S17(1)	Inverted tee	8.0	Hollow cored	1.2	13.0	4.0	4.0
S17(R)	H-shaped	8.0	Y- shaped	2.7	13.0	4.0	0.5
S18(1)	Inverted tee	10.0	Channel	1.2	10.0	4.7	4.0
S18(2)	Inverted tee	10.0	Channel	1.2	10.0	8.0	4.0
S18(R)	Inverted tee	10.0	Double tee	2.5	10.0	3.5	1.0
S19(1)	Rectangular	10.0	Hollow cored	1.2	17.0	3.0	4.5
S19(2)	Rectangular	10.0	Hollow cored	1.2	17.0	4.8	4.5
S19(R)	Rectangular	10.0	Hollow cored	1.2	17.0	3.6	0.5
S20(2)	Inverted tee	6.1	Double tee	2.5	15.0	6.0	4.0
S20(R)	Inverted tee	6.1	Double tee	2.5	15.0	5.0	1.5

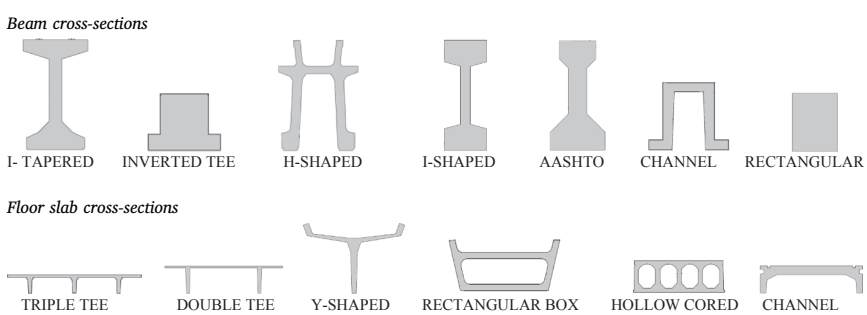

heights have been properly increased of same scale factor for the single-bay structures V1–V4, so obtaining structures with a first vertical period of 0.025 s, 0.050 s, 0.075 s and 0.10 s respectively. The four multi-bay virtual models, obtained accordingly, exhibiting vertical periods of 0.030 s, 0.057 s, 0.081 s and 0.11 s, respectively. In this way, the building stock selected covers a range of vertical periods from 0.025 s to 0.52 s. The natural periods are located in the portion of the vertical spectrum where the maximum acceleration amplification is expected, confirming that for this type of structures the vertical ground motion plays an important role in the seismic response.

Furthermore, due to the symmetry and regularity of the models, the natural modes vibrating with the highest mass percentage in the vertical direction are associated with a unison deformed shape. For some of the buildings, the authors considered also asymmetrical configurations, artificially created by introducing asymmetrical mass distributions or considering slightly different span length for beams.

From the comparison of outcomes from time-history analyses performed on symmetric and asymmetric models, the highest vertical fluctuations were provided by symmetrical models, resulting the worst condition from a structural point of view. Hence, the outcomes reported in the paper refer to symmetric models only.

4. Numerical analyses and results

4.1. Preliminary considerations

Interesting preliminary outcomes were obtained from the analysis of the vertical elastic frequencies and deformed shapes of the models, with recurring aspects exhibited by all structures.

Three natural vibration modes are usually sufficient to achieve an adequately high percentage of vertical vibrating mass, i.e. a modal participating mass ratio greater than 80%. The first natural vibration mode (i.e. the period with the highest percentage of vibrating effective mass) is typically related to flexural slab panel flexibility, whereas the second mode involves the beam flexibility and the third one the column axial flexibility. In some cases, first and second mode are condensed on a unique vibrating mode. In other cases, instead, they are switched in order. Furthermore, the axial flexibility of the columns is generally related to a mode with a limited percentage of vertical vibrating mass, ranging from 5% to 20% of the total mass and natural periods in the range 0.005–0.015 s.

Furthermore, from multi-storey structures in the building stock, we observed that generally, each storey vibrates vertically almost

Table 3
Main data on column details collected from as-built projects (R_{ck}: concrete cubic characteristic strength; (1): first floor in a multi-storey building; (2): second floor in a multi-storey building; (R): roof floor in a multi-storey building).

Structure	Cross-section (B × H) [cm]	Corner rebar [mm]	Intermediate rebar (along B; along H) [mm]	Stirrups [mm]	Rck [MPa]	Steel class
S1	40 × 70	∅26	2∅26; 3∅26	∅8@250	50	FeB44k
S2	60 × 60	∅24	5∅22; 5∅22	∅8@250	40	FeB44k
S3	70 × 70	∅22	1∅20; 1∅20	∅8@300	40	FeB44k
S4	60 × 60	∅26	2∅24; 2∅24	∅8@200	50	FeB44k
S5	40 × 70	∅24	2∅24; –	∅6@300	50	FeB44k
S6	50 × 50	∅20	2∅20; 2∅20	∅8@250	50	FeB44k
S7	60 × 70	∅22	2∅22; 4∅22	∅8@250	50	FeB44k
S8	70 × 70	∅24	3∅26 + 1∅20; 3∅26 + 1∅20	∅10@200 + 1hook ∅8@200	50	FeB44k
S9	50 × 50	∅22	2∅20; 2∅20	∅8@250	45	FeB44k
S10	60 × 60	∅22	2∅24; 2∅24	∅6@250	45	FeB44k
S11	65 × 75	∅22	1∅22; 1∅22	∅6@300	45	FeB44k
S12	60 × 60	∅22	2∅22; 2∅24	∅8@250	50	FeB44k
S13	55 × 55	∅24	1∅24; 1∅24	∅8@250	50	FeB44k
S14	55 × 55	∅30	1∅20; 1∅20	∅8@250	56	FeB32k
S15	50 × 50	∅18	1∅18; 1∅18	∅5@200	50	FeB32k
S16(1)	60 × 60	∅24	2∅22; 2∅22	∅8@250	40	FeB44k
S16(R)	60 × 60	∅24	2∅22; 2∅22	∅8@250	40	FeB44k
S17(1)	50 × 70	∅24	2∅24; 2∅24	∅8@250	50	FeB44k
S17(R)	50 × 70	∅24	2∅24; 2∅24	∅8@250	50	FeB44k
S18(1)	90 × 90	∅20	1∅20; 1∅20	∅8@250	45	FeB44k
S18(2)	70 × 70	∅20	1∅20; 1∅20	∅8@250	45	FeB44k
S18(R)	50 × 50	∅20	1∅20; 1∅20	∅8@250	45	FeB44k
S19(1)	60 × 60	∅18	3∅18; 1∅14	∅5@250	45	FeB44k
S19(2)	60 × 60	∅18	3∅18; 1∅14	∅5@250	45	FeB44k
S19(R)	60 × 60	∅18	3∅18; 1∅14	∅5@250	45	FeB44k
S20(1)	75 × 75	∅22	–; –	∅8@250	50	FeB44k
S20(2)	75 × 75	∅22	–; –	∅8@250	50	FeB44k
S20(R)	75 × 75	∅22	–; –	∅8@250	50	FeB44k

independently from the others. In fact, we distinguished different vibrating modes for the various storeys with each mode involving mainly just one storey. This aspect has been also observed and confirmed by the time-history analyses. From a practical point of view, each floor could then be studied in the vertical direction separately from the others.

In any case, it seems useful to highlight that safety judgement of precast building is typically based on the effects of the horizontal actions. Nevertheless, as far as the vertical to horizontal influence is concerned, in some studies on precast buildings hit by medium-low horizontal ground motions, the contribution of strong vertical excitation was proved to be crucial [66], decreasing in a considerable way the safety factor. So, in general, even if the estimation of seismic induced horizontal effects is typically the main goal of a procedure (for instance the seismic assessment or the safety judgment of a building), the strong vertical to horizontal influence should be considered in many cases.

The interaction in the reverse side (i.e. horizontal to vertical influence), is not always so strong, at least for RC precast structures with strong connection-weak column damage mechanism. In fact, with columns acting as cantilevers when subject to low-medium horizontal ground motions not activating the plastic capacity of the horizontal connections, structural damage is typically restricted to a limited portion of the total length of the columns (comparable with the plastic hinge length). Under this hypothesis, the response of the structure subject to ground motion in vertical direction experiences minor modification. As a result, for horizontal ground motions not activating the connections plastic capacity, seismic effects due to horizontal components results almost negligible when the vertical response of the structure subject to a vertical ground motion must be assessed. This outcome is further clarified by the results reported in Appendix A.

4.2. Response parameter definition

In order to assess the behaviour of this particular class of RC precast structures when subject to vertical ground motion, the seismic fluctuations of vertical forces, recorded at the extremities of beams and floor slab elements (i.e. seismic vertical shear forces), are investigated. The fluctuations of shear forces recorded at the extremity are, for equilibrium reason, also fluctuations of column axial forces. The aim is pursued by time-history analyses performed on the 48 FE models (24 single-bay models and 24 multi-bay models depicted in Fig. 3), subject to the selected vertical ground motions, in order to evaluate the structural response for earthquakes of different intensity (with PGA_V used as the intensity measure). The numerical outcomes are expressed in terms of dimensionless parameter α defined as the ratio between vertical force induced by seismic action (F_{SEIS}) and the vertical force due to gravitational loading (F_{GR}):

$$\alpha = |F_{SEIS}/F_{GR}| \tag{1}$$

The procedure to obtain the ratio α to be attributed to a general storey of the structures is depicted in Fig. 5 with reference to beam elements. If n is the number of ground motions of the subset, and m is the number of end sections of the beams of the considered storey, a value $\alpha_{i,j}$ was computed for each end section i (with $i = 1,\ldots,n$) and for every ground motion j (with $j = 1,\ldots,m$), by selecting the peak value from the corresponding α time-series obtained from the time-history analyses, so obtaining $m \times n$ values of α. In the second stage, the average values $\bar{\alpha}_1, \cdots, \bar{\alpha}_m$ were calculated with reference to each end section and, finally, the maximum value (named α_{max}), between the $\bar{\alpha}_1, \cdots, \bar{\alpha}_m$ ratios, was selected and attributed to the storey. In this way, the obtained α_{max} ratio can be considered an estimate of the maximum value of the vertical force ratio for the considered storey.

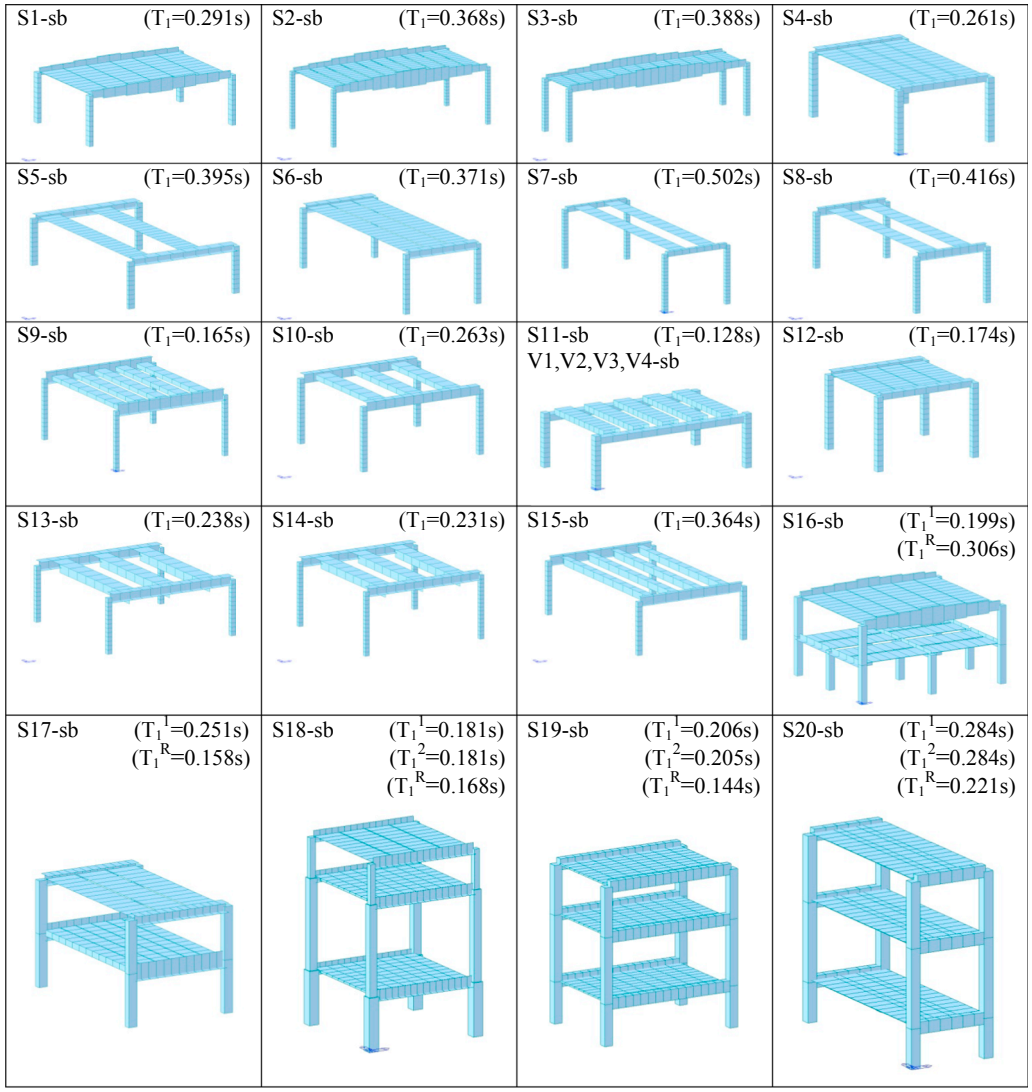

(a)

Fig. 3. The building stock of precast structures considered in the study. Three-dimensional numerical FE models: (a) Single-bay (sb) models; (b) Multi-bay (mb) models. T_1 indicates the first vibrating vertical period of each storey in the building (with [1]: first floor in a multi-storey building; [2]: second floor in a multi-storey building; [R]: roof floor in a multi-storey building).

4.3. Numerical results

4.3.1. Far Fault (FF) seismic input

The main outcomes of the time-history analyses conducted on the 48 FE models (24 single-bay and 24 multi-bay structures) subject to the ground motions of the four far fault (FF) subsets defined in Section 2 are reported in the present Section. Fig. 6a shows, the values of the maximum vertical force ratio α_{max} for the perimeter beam belonging to one of the storey, considering the various storeys as independent in case of multi-storey buildings. 64 α_{max} values, one for each of the independent storey, were computed (32 from single-bay models and 32 from multi-bay models). They are plotted in the figure as a function of the vertical elastic period associated with the first natural mode of each storey. α_{max} calculated for internal beams (32 values from multi-bay models) and floor slab elements (64 values of α_{max}) respectively are shown in Fig. 6b and c. The value $\alpha_{max} = 1$ in the figures indicates a maximum value of seismic vertical force equal to the static gravitational vertical force (i.e. the summation of self-weight, dead and live loads in seismic combination).

The larger values obtained for floor slab elements highlight their greater sensitivity to vertical excitations. Peaks of vertical force fluctuations lay in the period range 0.05–0.15 s. In that range, for PGA_V greater than 0.5*g*, $\alpha_{max} > 1$ indicates that the vertical seismic force overcomes the static gravitational force. Hence, both beams and floor slab elements tend to lift up from the supports. If no mechanical connections are present, as in the case of structures designed without seismic provisions, also smaller values of α can be very dangerous, because a reduction of vertical force at the support level reduces the friction force representing the resistance against loss of support.

4.3.2. Near Fault (NF) seismic input

With regard to each of the five near fault (NF) excitation subsets, α_{max} obtained for beams (both perimeter and internal) and floor slab elements are shown in Fig. 7, versus the first vertical natural period *T* of each storey. The values of parameter α_{max} are greater than the ones obtained from FF records for the periods around 0.1 s. For periods greater than 0.1 s, in general, NF records produce vertical effects smaller than FF records with the latter, characterized by different frequency content, able to produce a greater excitation for the longer periods. Again, the most sensitive elements to vertical motion appear to be the floor slab elements and also in this case, in the period range 0.05–0.15 s. For PGA_V greater than 0.5*g*, the seismic force overcomes

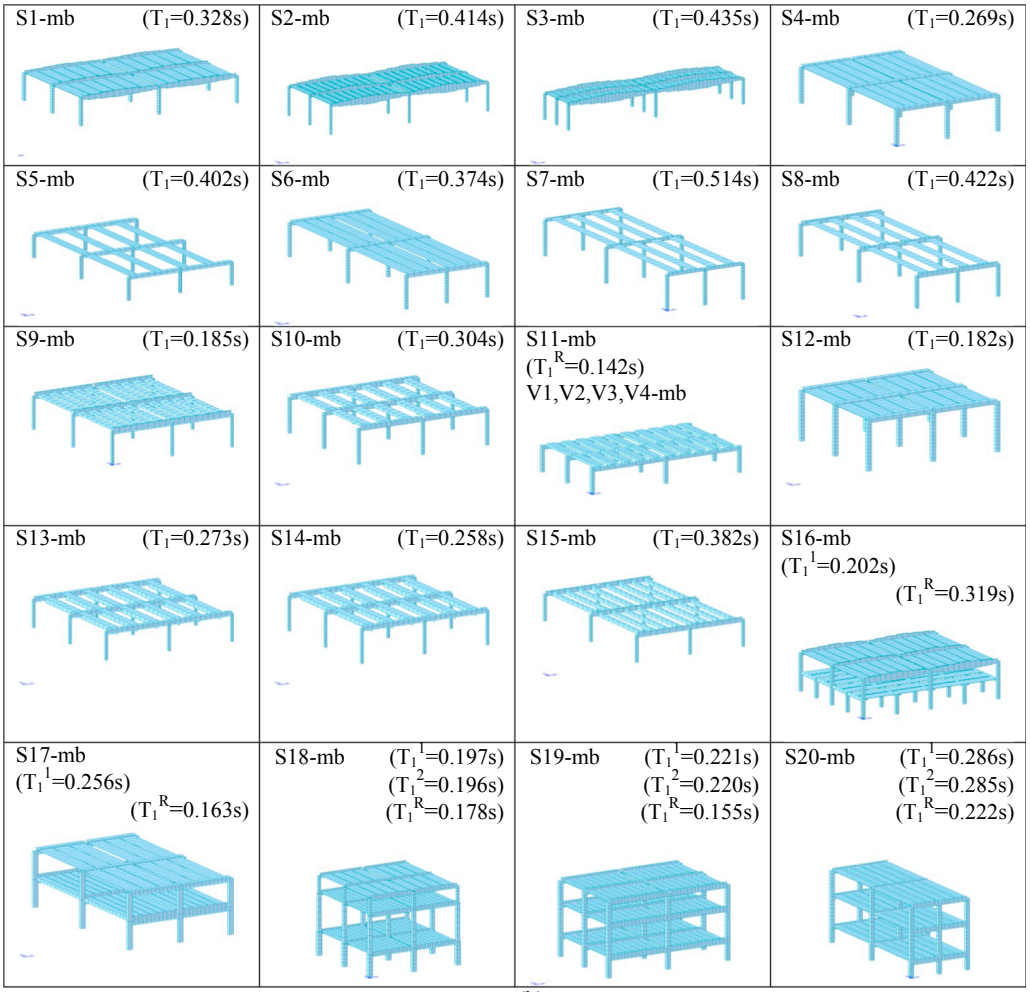

(b)

Fig. 3. (*continued*)

the gravitational force for beams and floor slab elements. Conversely, when the seismic force acts downwards, due to the high values of α_{max}, a significant increase of the axial force in the columns is expected. This phenomenon may occur also in low-seismicity areas. For example, in geographical regions where the estimated PGA_V lies in the range 0.1–0.2*g* or 0.2–0.4*g*, for a structure with a first vertical period of 0.1 s, the increase of the axial force in the internal columns due to seismic action is 40% and 75%, respectively; for perimeter columns the increase of axial force is around 45% and 85% respectively. Section ductility of columns subject to horizontal forces is, consequently, significantly reduced.

4.3.3. Pulse-Velocity (PV) seismic input

One of the aspects clarified in several studies, and confirmed by the analysis of the accelerations recorded in recent earthquakes, is that horizontal components of near fault ground motions usually present

Table 4
Values of coefficients a_1, a_2, a_3, b_1, b_2, b_3, c_1, c_2, c_3, d_1 and d_2 in Eqs. (4) and (5) obtained from the nonlinear regression analysis of time-histories outcomes for near fault (NF) and far fault (FF) excitation, for perimeter beams, internal beams and floor slab elements. R^2 is the coefficient of determination obtained for the various elements.

Coefficient	Near fault (NF) excitation			Far fault (FF) excitation		
	Perimeter beam	Internal beam	Floor slab	Perimeter beam	Internal beam	Floor slab
a_1 [s^{-2}]	766.93	−56.99	313.83	128.76	100.40	1190.40
a_2 [s^{-2}]	−690.98	−53.95	−415.48	−134.13	−106.14	−1256.40
a_3 [s^{-2}]	−108.86	−91.09	−8.48	−197.08	−117.07	75.63
b_1 [s^{-1}]	−184.25	−19.75	−100.45	−29.34	−26.69	−260.65
b_2 [s^{-1}]	158.57	30.58	106.22	31.00	27.21	275.74
b_3 [s^{-1}]	16.79	13.63	−1.90	35.29	19.91	−20.58
c_1 [/]	10.63	3.43	7.47	1.27	1.46	12.87
c_2 [/]	−8.84	−3.27	−6.93	−1.49	−1.47	−13.64
c_3 [/]	1.44	2.12	3.35	0.59	1.72	4.21
d_1 [/]	0.17	0.30	0.35	−0.16	−0.09	−0.06
d_2 [/]	0.29	0.74	0.87	0.54	1.01	1.07
R^2 [/]	0.90	0.88	0.86	0.93	0.90	0.86

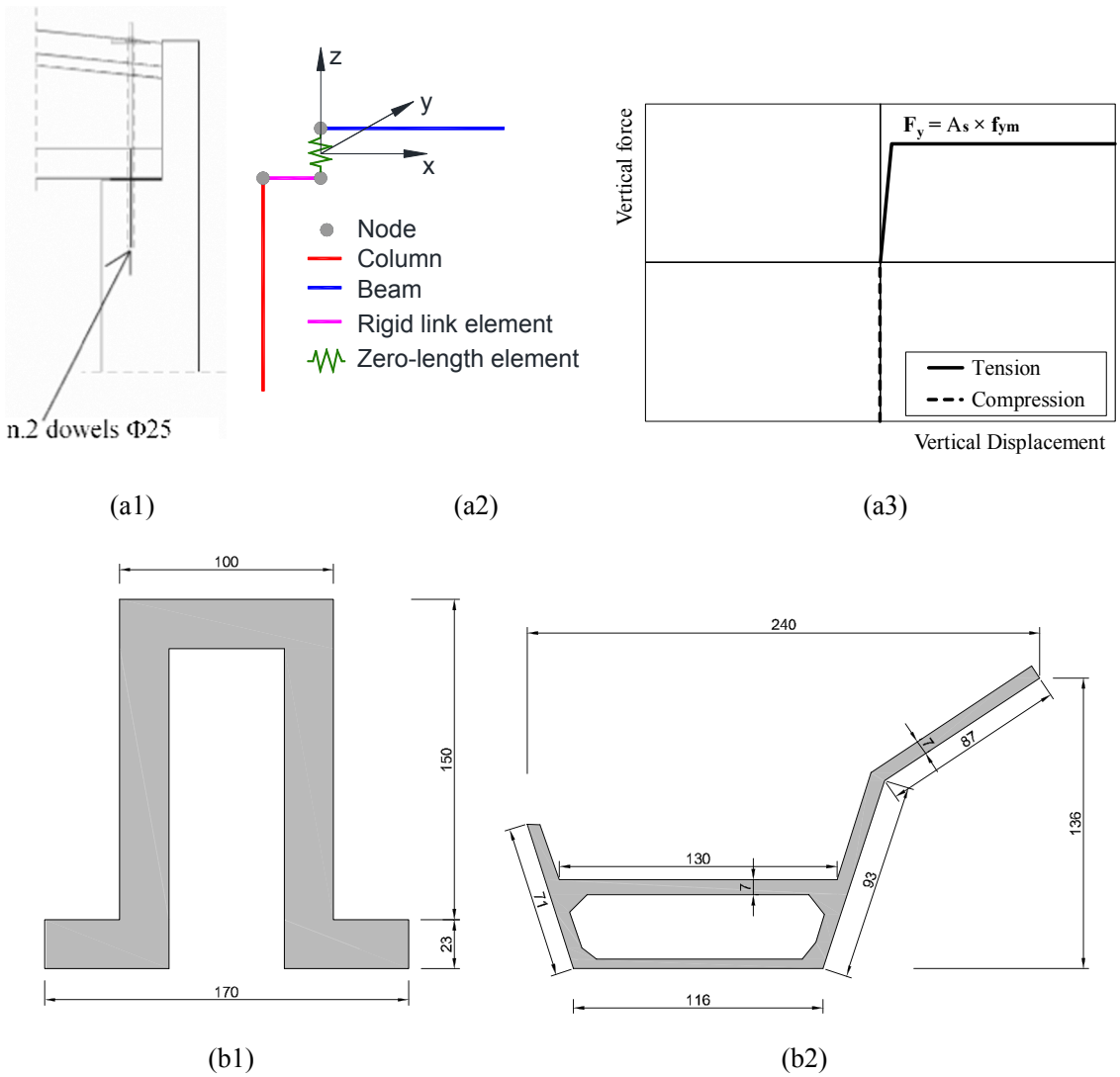

Fig. 4. Details adopted in structure modelling. (a) Modelling of a beam-column connection. (a1) Example of a real structural configuration as resulting from the as-built design and (a2) numerical FE model. (a3) Nonlinear behaviour assumed for the zero-length element in vertical (z-) direction. (b) Cross-section of typical horizontal elements of structure S11 (measures are in cm). (b1) Beams, (b2) Roof slab elements.

high peak ground velocity (PGV_H) with pulse-velocity shape [67,68]. Furthermore, with regard to horizontal ground motions, some studies demonstrated that, for near fault earthquakes, peak ground velocity is a better indicator of seismic damaging potential than peak ground acceleration [69]. Strong near fault motions are often characterized by pulse-velocity records also in vertical direction [70–72].

In the following, we will show that pulse-velocity vertical records produce seismic forces in precast structures greater than non-pulse-velocity ground motions. In this study, the vertical PV components were prescribed to the base of single-bay FE models of the buildings stock. Vertical fluctuations of the column axial forces and reaction at the supports (the extremities of beams and floor slab elements) were obtained from nonlinear dynamic analyses. The values of α_{max} obtained for perimeter beams and floor slab elements are reported in Fig. 8, where results from near fault (NF) and pulse-velocity (PV) ground motions for the three subsets with different seismic intensity levels (PGA_V) are compared. Furthermore, Fig. 9 shows the ratio α_{max}(PV)/α_{max}(NF), i.e. the ratios between α_{max} obtained, for the same storey, adopting pulse-velocity α_{max}(PV) and near fault α_{max}(NF) subsets characterized by analogous PGA_V. For both beams and floor slab elements, the tendency of the near fault pulse-velocity motions is to produce, on precast buildings, vertical effects greater than those due to near fault records without pulse-velocity shape.

In Fig. 9, the linear regression equations for the various seismic intensity subsets are also reported. A clear correlation is found between the increase of vertical forces and vertical period of structures in the range 0.01–0.6 s, more significant for the lowest seismic intensities. Even though a reliable and undoubted relation between these data is difficult to establish, the increase of vertical forces in the case of pulse-velocity ground motions is undeniable. This aspect will be the subject of more detailed analyses in future studies.

4.3.4. Seismic intensity measures and correlation with vertical force fluctuations

In order to establish the best seismic indicator correlated with the vertical force fluctuation, three seismic intensity measures were considered in the present study: vertical peak ground acceleration (PGA_V), vertical peak ground velocity (PGV_V) and vertical peak spectral acceleration (PSA_V). As a measure of the vertical force fluctuations, α_{max} was adopted, which is directly correlated to most of the structural issues connected to variations of the vertical force at the level of beam-column supports (i.e. increase of compression axial column forces, column shear strength reduction, column ductility reduction, tensile force in the mechanical devices of connections).

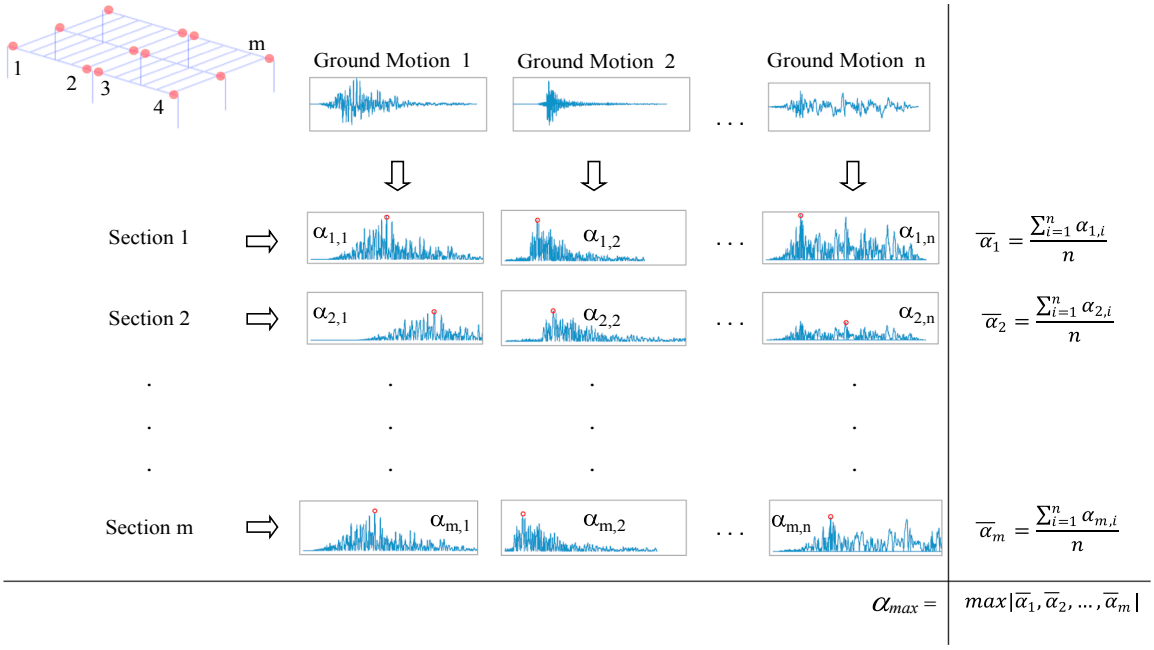

Fig. 5. Procedure adopted for post-processing of time-history results to obtain α_{max} of a general storey.

As an example, but with general validity, Fig. 10 shows the correlation between the three intensity measures and values of α_{max} obtained from FE model of precast structures subject to FF, NF, PV ground motions. In particular, perimeter beams, internal beams and floor slab elements of three different structures of the stock building (the multi-bay S1, S9 and V4 structures, with first vertical period of 0.33 s, 0.19 s and 0.11 s respectively), subjected to the 30 vertical components of the seismic excitations described in Appendix A, are considered. The ground motion subsets were constituted by 10 near fault, 10 far fault and 10 pulse-velocity records, respectively, covering wide ranges of PGA_V, PGV_V and PSA_V. Details on the adopted selection criteria are reported in Appendix A. The results clearly show that PGA_V and PGV_V are not well correlated with α_{max} ratio, resulting very poor predictors of the maximum vertical force fluctuations induced by the earthquake. On the opposite side, PSA_V seems an excellent predictor of the seismic vertical force fluctuations. The reason for the high correlation between PSA_V and parameter α_{max} is mainly due to the quasi-elastic behaviour exhibited by this class of structures (with regards to vertical excitation) with damaging phenomena, mainly affecting columns, scarcely influencing the vertical response of the storeys, constituted by simply-supported beams and floor slab elements vibrating substantially in the elastic range.

5. Analytical expression for α_{max} prediction

By analysing outcomes from nonlinear time-histories (detailed in Section 4), and in particular the variation of dimensionless parameter α_{max} for increasing values of T, i.e. $\alpha_{max}(T)$, three different branches can be defined. As boundary points of the three identified portions, the values of $T_B = 0.05$ s and $T_C = 0.15$ s prescribed by EC8 for the definition of vertical acceleration spectra were adopted. The best fitting of numerical results, pursued by a nonlinear regression, was done by imposing, for the three portions, a first piecewise linear relation followed by a quadratic polynomial and a hyperbolic function. The analytical expression proposed for $\alpha_{max}(T)$ has the form:

$$\alpha_{max}(T) = \begin{cases} \left(1 - \frac{T}{0.05} + \beta_{0.05} \cdot \frac{T}{0.05}\right) \cdot \frac{PGA_V}{g} & for \quad T < 0.05 \ \text{s} \\ \beta(T, PGA_V) \cdot \frac{PGA_V}{g} & for \quad 0.05 \ \text{s} \le T < 0.15 \ \text{s} \\ \beta_{0.15} \cdot \left(\frac{0.15}{T}\right)^{\gamma} \cdot \frac{PGA_V}{g} & for \quad T \ge 0.15 \ \text{s} \end{cases} \tag{2}$$

where g (in mm/s^2) is the gravity acceleration, PGA_V (in mm/s^2) denotes the peak ground vertical acceleration, T is the vertical period of the structure for single-storey buildings or, in the case of multi-storey buildings, the vertical period with the higher percentage of vertical vibrating mass for the storey of interests. Moreover, β (T, PGA_V) and γ (PGA_V) are two dimensionless functions to be calibrated, for which the following expressions were selected:

$$\beta(T, PGA_V) = a(PGA_V) \cdot T^2 + b(PGA_V) \cdot T + c(PGA_V) \tag{3}$$

$$\gamma(PGA_V) = d_1 \cdot \frac{PGA_V}{g} + d_2 \tag{4}$$

where

$$\begin{cases} a(PGA_V) = a_1 \cdot (\frac{PGA_V}{g})^2 + a_2 \cdot (\frac{PGA_V}{g}) + a_3 \\ b(PGA_V) = b_1 \cdot (\frac{PGA_V}{g})^2 + b_2 \cdot (\frac{PGA_V}{g}) + b_3 \\ c(PGA_V) = c_1 \cdot (\frac{PGA_V}{g})^2 + c_2 \cdot (\frac{PGA_V}{g}) + c_3 \end{cases} \tag{5}$$

Coefficients a_1, a_2, a_3, b_1, b_2, b_3, c_1, c_2, c_3, d_1 and d_2 in Eqs. (4) and (5) were identified via nonlinear regression analysis. They are reported in Table 4 for the two excitation types (Far Fault and Near Fault) and for the three types of structural elements (perimeter beam, internal beam and floor slab) considered in the present study. The coefficients of determination R^2 between numerical and analytical outcomes are reported in Table 4 for the various cases and range from 0.86 to 0.93. Moreover, coefficients $\beta_{0.05}$ and $\beta_{0.15}$ in Eq. (2) are the values of function β for $T = 0.05$ s and 0.15 s, i.e.:

$$\beta_{0.05} = \text{a}(PGA_V) \cdot 0.05^2 + \text{b}(PGA_V) \cdot 0.05 + \text{c}(PGA_V) \tag{6a}$$

$$\beta_{0.15} = \text{a}(PGA_V) \cdot 0.15^2 + \text{b}(PGA_V) \cdot 0.15 + \text{c}(PGA_V) \tag{6b}$$

Lastly, in order to compare expressions of α_{max} for the various ground motion subsets, the no dimensional parameter α_{max}^* is defined:

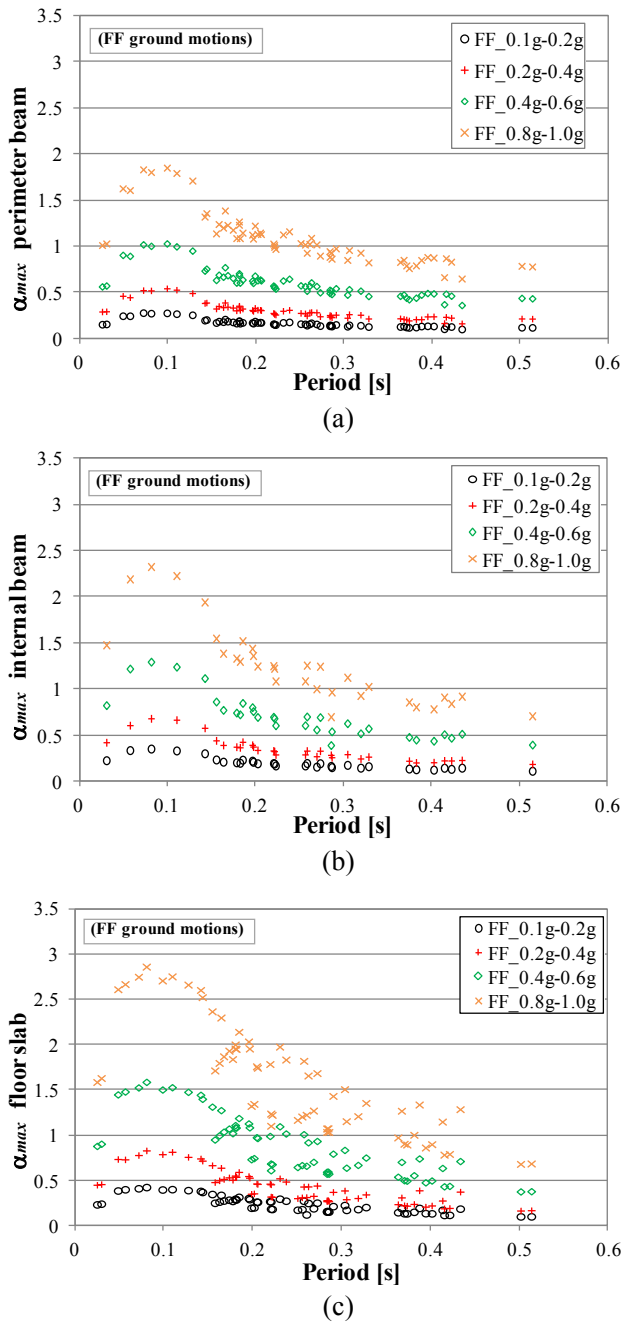

Fig. 6. α_{max} obtained for the four Far Fault (FF) ground motion subsets considering the 64 independent storeys (32 from single-bay models and 32 from multi-bay models) identified by their vertical vibration periods. α_{max} are calculated at the extremity cross-sections of: (a) perimeter beams; (b) internal beams (from multi-bay models); (c) floor slab elements.

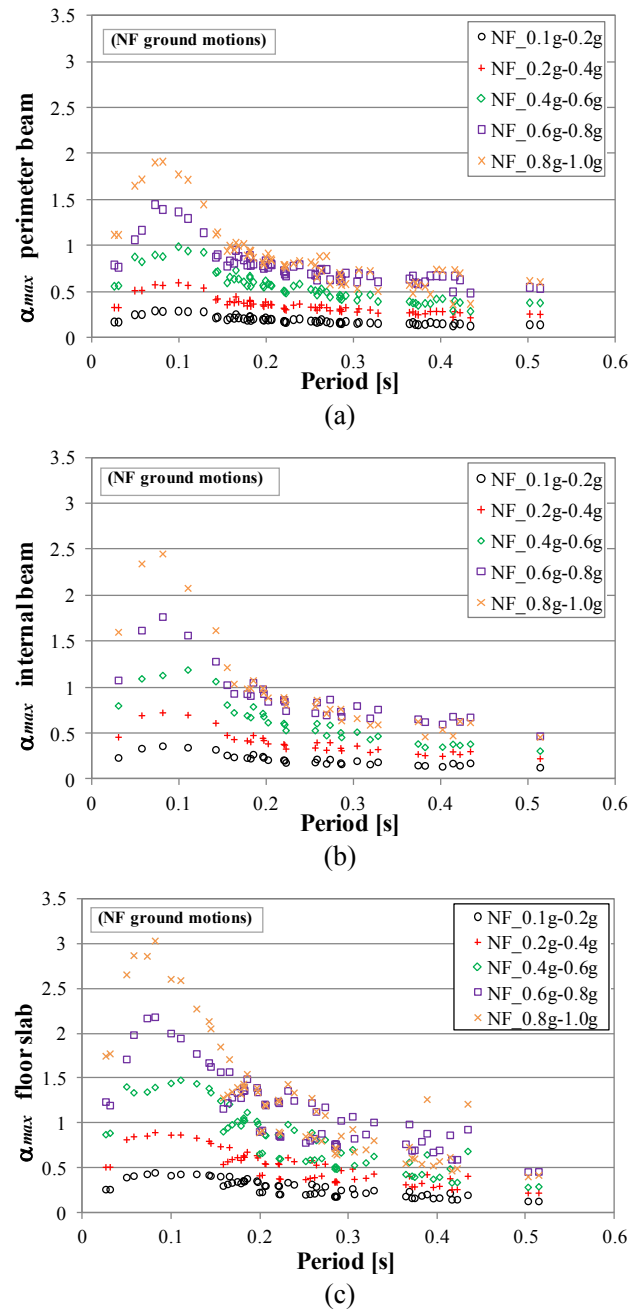

Fig. 7. α_{max} obtained for the five Near Fault (NF) ground motion subsets considering the 64 independent storeys (32 from single-bay models and 32 from multi-bay models) identified by their vertical vibration periods. α_{max} are calculated at the extremity cross-sections of: (a) perimeter beams; (b) internal beams (from multi-bay models); (c) floor slab elements.

$$\alpha_{max}* = \alpha_{max} \cdot g / PGA_V \tag{7}$$

From the analytical expression in Eq. (2), the trends of α_{max}^* are depicted in Fig. 11, for different PGA_V levels and with reference to the near fault excitation type. Figures show that, with the increase of the seismic intensity, the vertical force fluctuations increase for $T < 0.15$ s, while they decrease for longer periods. Moreover, comparing α_{max}^* values in Fig. 11a–c, it is evident that the floor slab elements are subject to vertical force fluctuations greater those of beams.

Fig. 12 shows the variation of parameter α_{max}^* for perimeter beams, internal beams and floor slab elements for different PGA_V levels, but considering the FF excitation type. Analogous conclusion as before can be drawn, with floor slab elements more sensitive to vertical excitation than beams. Parameter α_{max}^* for NF and FF records shows similar trends, with FF records having smaller peak values (around the period of 0.1 s) but higher values for long periods (from 0.1 s to 0.6 s).

Fig. 13 reports an interesting comparison between results coming from time-history analyses, analytical expression in Eq. (2) and response spectral analyses with EC8 provisions, i.e., performing response spectral analyses with a behaviour factor $q = 1.5$ for vertical accelerations. Two different seismic intensity levels, measured in terms of $PGAv$, have been considered. Assuming a value $PGAv = 0.147g$ (where

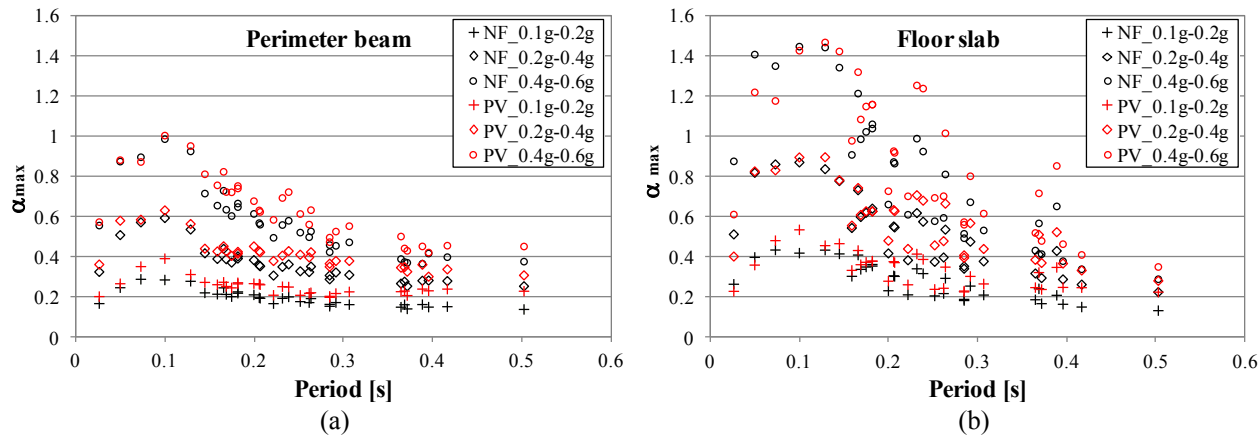

Fig. 8. α_{max} obtained, for the 32 independent storeys identified by their vertical vibration periods, considering three subsets of Near Fault (NF) and Pulse-Velocity (PV) ground motions: (a) Perimeter beams; (b) Floor slab elements.

the value represents the mean value of the *PGAv* of the 189 records of the NF subset with *PGAv* in the range 0.1–0.2*g*), the trend of analytical expression has been computed. For the response spectral analysis a vertical acceleration response spectrum was adopted, defined following the EC8 provisions, assuming $PGAv = 0.147g$, $T_B = 0.05$ s, $T_C = 0.15$ s, $T_D = 1.0$ s and $\eta = 1.0$. The results for this level of seismic intensity are reported in Fig. 13a.

An analogous procedure has been adopted for the higher level of seismic intensity. In this second case, the value of *PGAv* adopted is equal to 0.287*g* (where the present value represents the mean value of the *PGAv* of the 127 records of the NF subset with *PGAv* in the range 0.2–0.4*g*). The response spectrum EC8 compliant has been then updated to the new value of *PGAv*. The results of the analyses considering the higher level of *PGAv* are reported in Fig. 13b.

The emerging outcomes show that, for design purpose, the latter systematically underestimates vertical force fluctuations obtained by time-histories.

This important finding suggests that the use of spectral response analysis, with the actual design spectra, in accordance to several international building codes could underestimate the vertical force fluctuations induced by the earthquake. Underestimation can be due to the adoption of $q = 1.5$, because precast roof elements behave substantially elastically when subject to vertical motion. No vertical element reached yielding deformation on rebars or along the element length for the seismic excitation considered in the present study (vertical excitation only). Of course, horizontal excitation produces large bending moments in columns, whereas their effect in connection rebars is negligible.

It is worth noting that, according to the results presented in this paper, α_{max} has the best correlation with PSA_V, being the latter the spectral acceleration of the spectrum related to the recorded accelerograms adopted in the present study. Nevertheless, the analytical expression proposed in Eq. (2) is guided by design purposes, where typically the PGA_V at the site is known and the non-dimensional shape of elastic spectrum for vertical acceleration proposed by the codes (e.g. Eurocode) is adopted. Nevertheless, the preliminary outcomes of this study indicate a poor correlation between the non-dimensional shape of elastic spectrum for vertical acceleration proposed by international codes and the spectrum of recorded vertical ground motions (see for instance Fig. 2). Hence, if PSA_V, estimated from the codes, is introduced in Eq. (2), significant errors in the evaluation of α_{max} can be expected. For this reason, the authors proposed here an analytical expression requiring, in the design phase, the minimum number of parameters to define the demand due to seismic excitation, i.e., only the PGA_V. The β function introduced in Eq. (3) has the role of expressing the dependence on the natural period in a way which is more accurate than adopting the vertical spectrum proposed by codes. The analytical expression reported in Eq. (2) can be used in design to predict the maximum value of the vertical force fluctuations without the need of performing complex time-history analyses. Validation through a case study is documented in the following section.

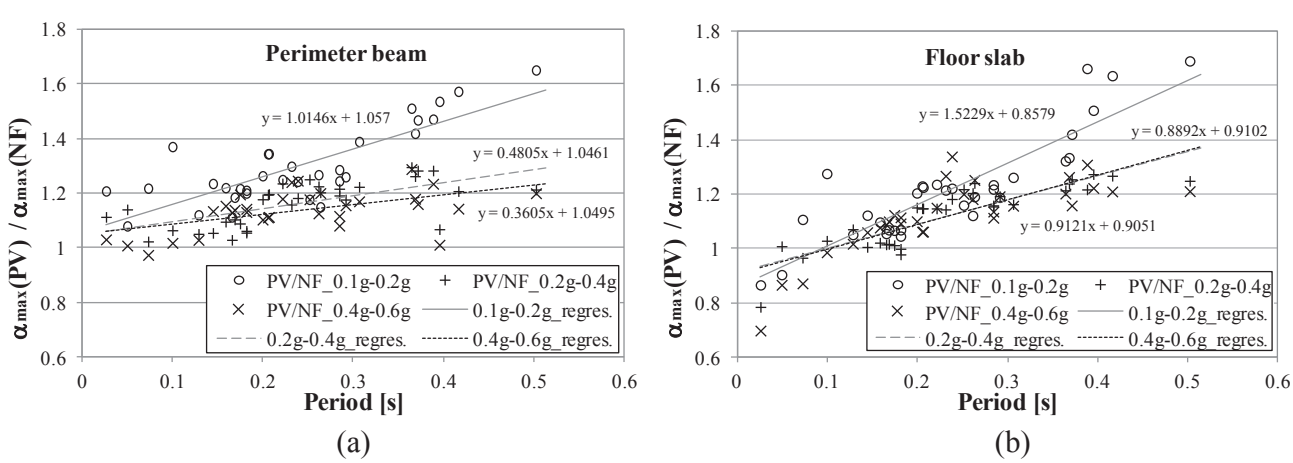

Fig. 9. Ratio α_{max}(PV)/α_{max}(NF), with α_{max}(PV) obtained from pulse-velocity records and α_{max}(NF) from near fault records. Values attained for various vertical seismic intensity intervals for: (a) perimeter beams; (b) floor slab elements. Solid and dashed lines indicate regression curves for different PGA_V intervals.

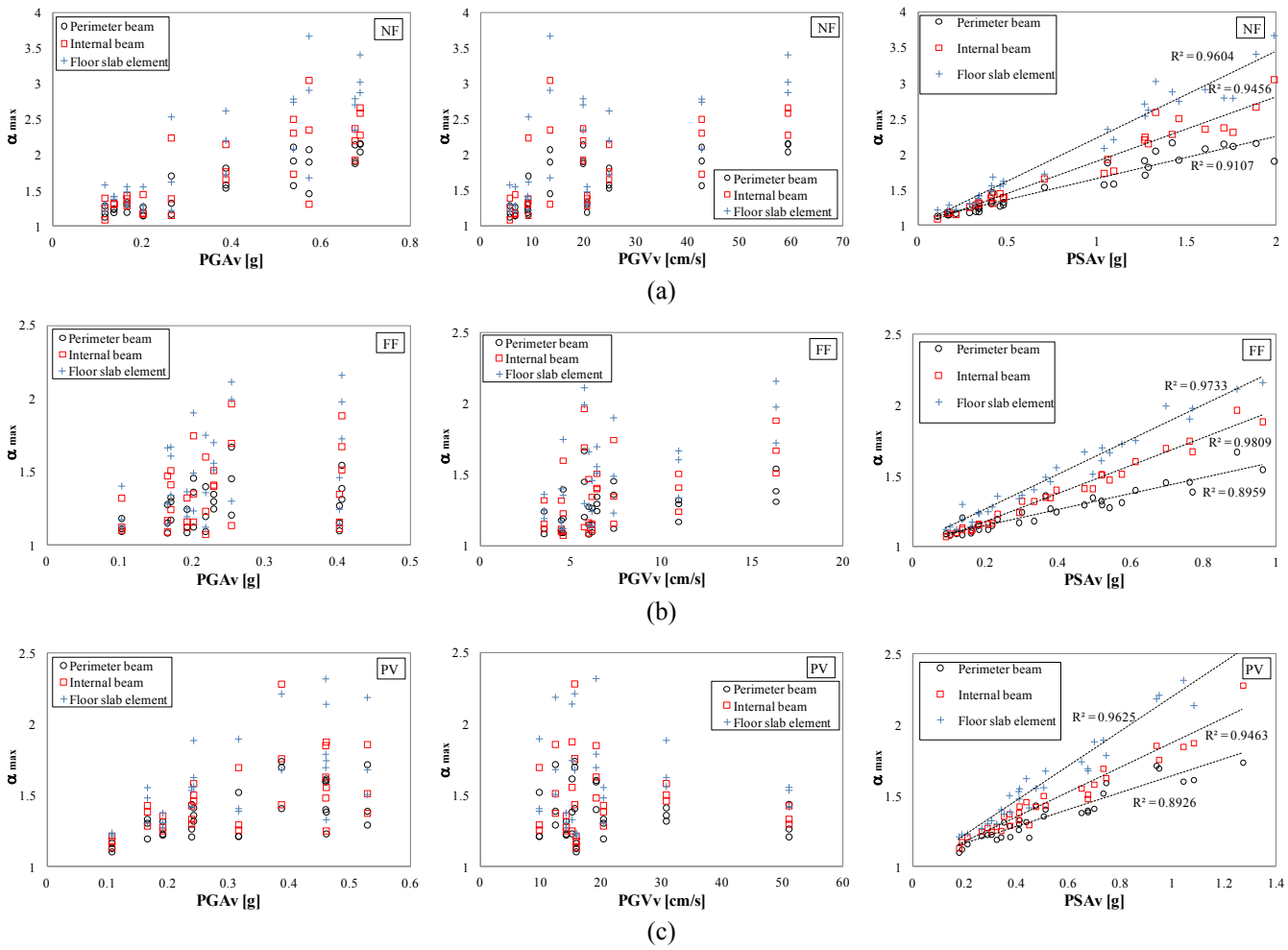

Fig. 10. Correlation between α_{max} and the three seismic intensity measures PGA_V, PVA_V, PSA_V obtained from time-history analyses on the three structures S1, S9, V4 and considering the 30 seismic vertical records described in Appendix A (with 10 Near Fault, 10 Far Fault and 10 Pulse-Velocity excitation types): (a) Correlation for NF excitations; (b) Correlation for FF excitations; (c) Correlation for PV excitations.

6. Validating case study

For validation, the expression proposed in Eq. (2) was adopted for the evaluation of the vertical force fluctuation on a precast building not considered in the building stock used for calibration. Built in 1980 and located in Bastiglia (Modena) in the North-East of Italy, the structure is a single-storey RC building, with a height of 7.0 m from the ground level to the roof, 7 × 2 bays, respectively, of 4.85 m + 6 × 6.10 m in the longitudinal direction and 2 × 18.0 m in the transverse direction. Perimeter and inner columns have cross-sections of 40 × 40 cm and 40 × 50 cm, respectively. The roof storey is constituted by I-tapered beams in the transverse direction supporting the hollow core floor slab elements in the longitudinal direction of the building (for reference to cross-sections nomenclature see Table 2). Property of the materials (class of concrete and steel), reinforcement longitudinal bars and stirrups, dead and live loads, are those reported in the original design documentation of the building. Fig. 14 shows an aerial view of the building and the global FE model. The inelastic material laws and the type of finite element adopted are the same already described in Section 3.2. The first vertical natural period T of the structure, required in Eq. (2) for the evaluation of α_{max} is $T = 0.21$ s with a modal participating mass ratio of 65%.

Parameter α_{max} was evaluated for all the elements constituting the roof storey (i.e. perimeter beams, internal beams and storey slab elements), for a value of PGA_V equal to 0.3g. From Eqs. (2)–(6) and making use of coefficients of Table 4, α_{max} for each structural element was determined for both near fault and far fault excitation type. The values of α_{max} obtained from the analytical expression proposed in Eq. (2) were then compared with the results of a series of nonlinear time-history analyses conducted on the global FE model. As far as the vertical seismic excitation is concerned, 20 ground motions were selected and scaled in terms of PGA_V to a common value of 0.3g. Fig. 15 shows the comparison, for both types of seismic input, obtained from the analytical model and from time-histories with the procedure depicted in Fig. 5. Black circles indicate the values of α ratios obtained from the 10 ground motions considered, red hyphens their average, black cross the predicted value from Eq. (2).

The figure shows that the values estimated from the analytical model are in very good agreement with the average values of results from time-history analyses.

7. Concluding remarks

The paper reports the main outcomes of a research on the dynamic behaviour of single-bay and multi-bay existing strong connection-weak column RC precast buildings subject to the vertical excitation component of earthquakes. The buildings have precast storey elements with hinged connections. Time-history analyses were performed on 48

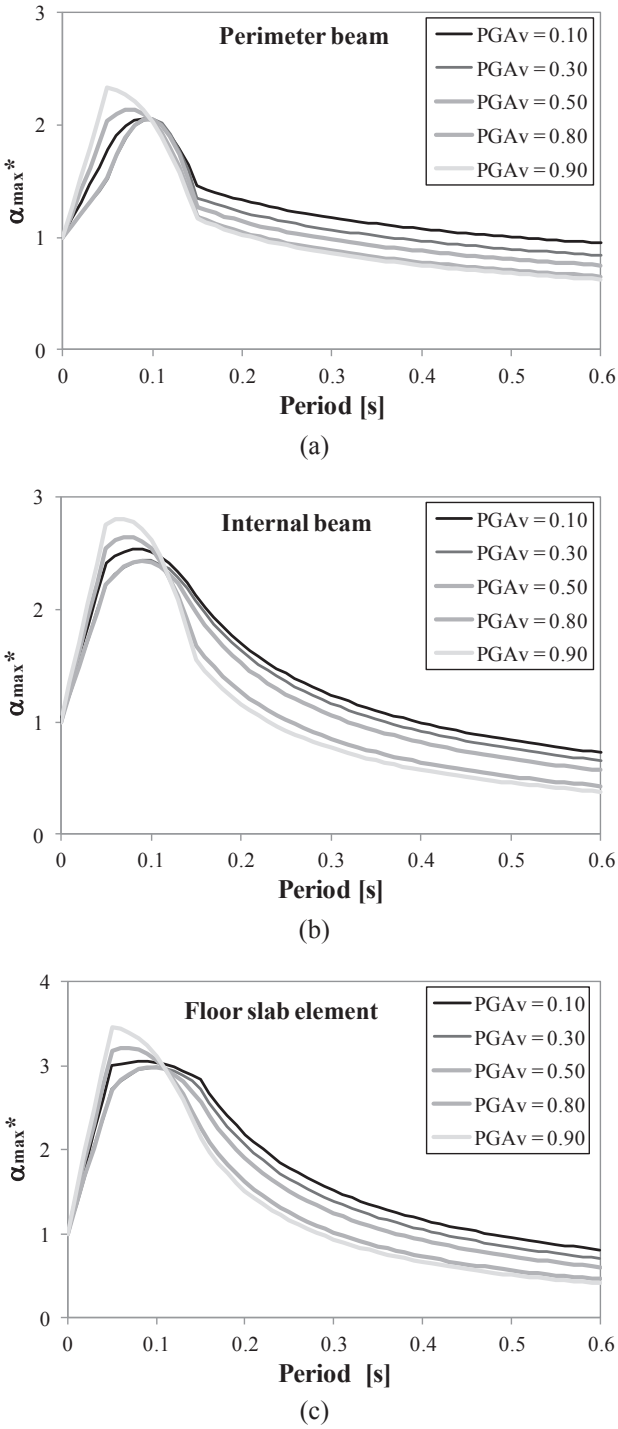

Fig. 11. Trends of α_{max}^{*} parameter, defined in Eq. (7), for near fault (NF) ground motions as a function of PGA_V levels: (a) Perimeter beams; (b) Internal beams; (c) Floor slab elements.

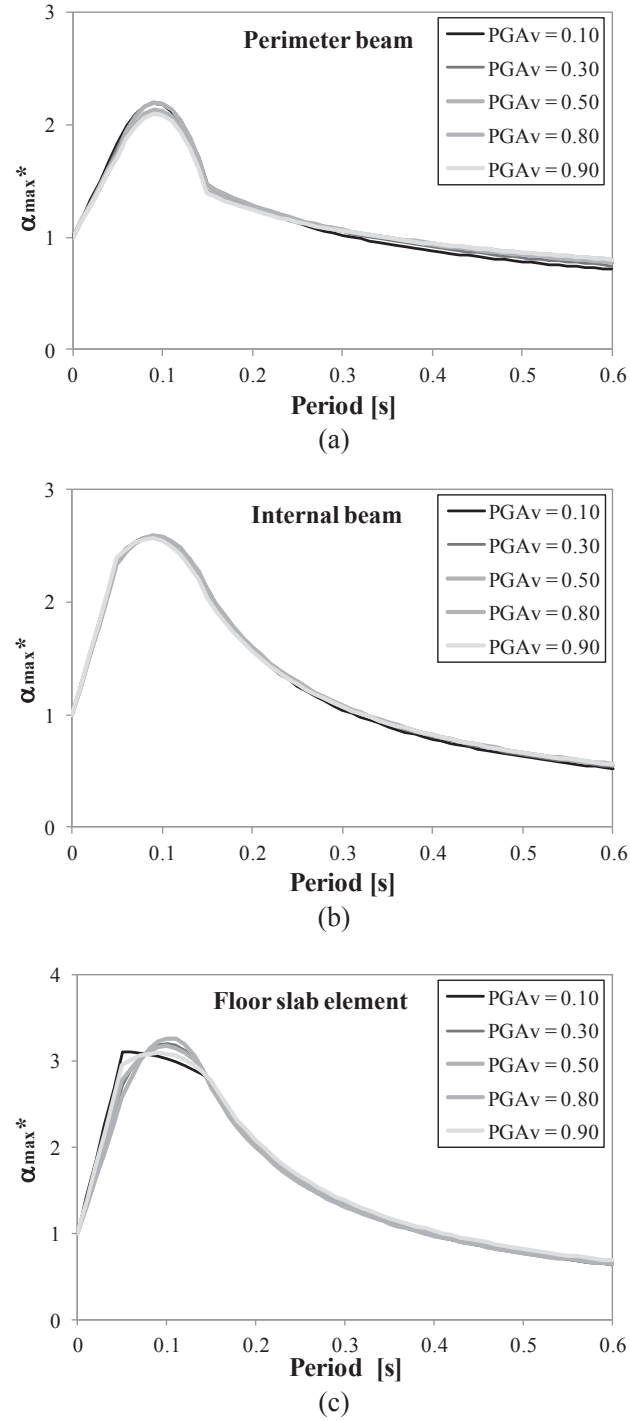

Fig. 12. Trends of α_{max}^{*} parameter, defined in Eq. (7), for far fault (FF) ground motions as a function of PGA_V levels: (a) Perimeter beams; (b) Internal beams; (c) Floor slab elements.

nonlinear FE models of precast structures for different levels and types of seismic excitation. The different seismic responses induced by near fault and far fault excitations were studied by selecting specific sets of ground motion records. Near fault records with pulse-velocity shape were also adopted in order to assess possible amplification of the seismic demand.

The numerical outcomes were expressed in terms of a synthetic parameter α_{max} expressing, for a specific storey, the maximum ratio between vertical force induced by seismic load and vertical force due to gravitational load in seismic combination for different types of structural elements. To this regard, the ratio α_{max} was obtained for perimeter beams, internal beams and floor slab elements. For the three types of elements, significantly different results were registered.

An analytical expression for α_{max} was then proposed and defined as a function of PGA_V and T (i.e., vertical peak ground acceleration and vertical first natural period of the storey/building), whose parameters were defined by nonlinear regression of numerical results. Comparison with EC8 provisions for design purpose, i.e. performing response

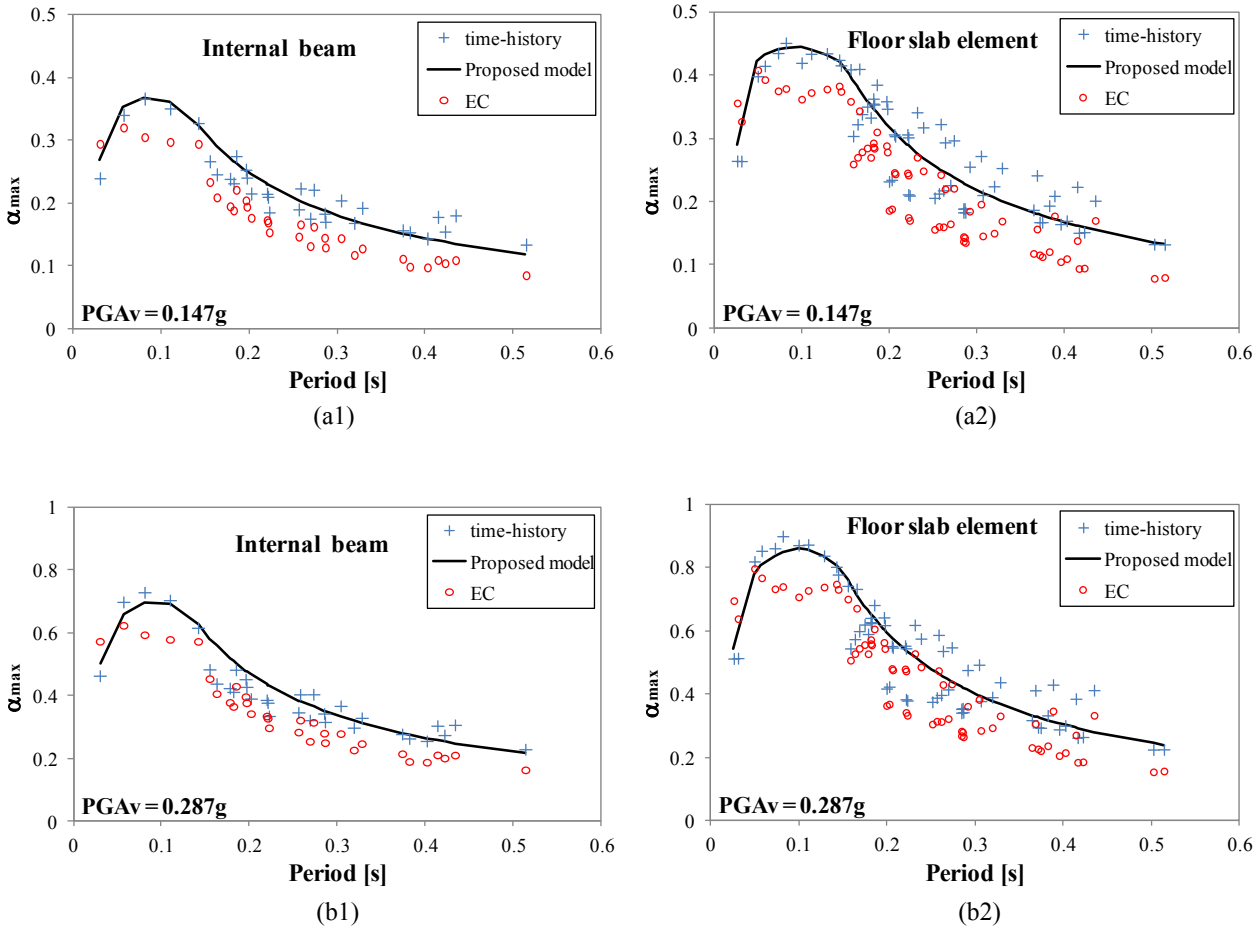

Fig. 13. α_{max} obtained via time-history analyses considering near fault (NF) excitations, compared with the analytical expression proposed in Eq. (2) and results obtained by response spectra analyses with EC8 spectrum: (a1) Results for internal beams for $PGA_V = 0.147g$; (a2) Results for floor slab elements for $PGA_V = 0.147g$; (b1) Results for internal beams for $PGA_V = 0.287g$; (b2) Results for floor slab elements for $PGA_V = 0.287g$.

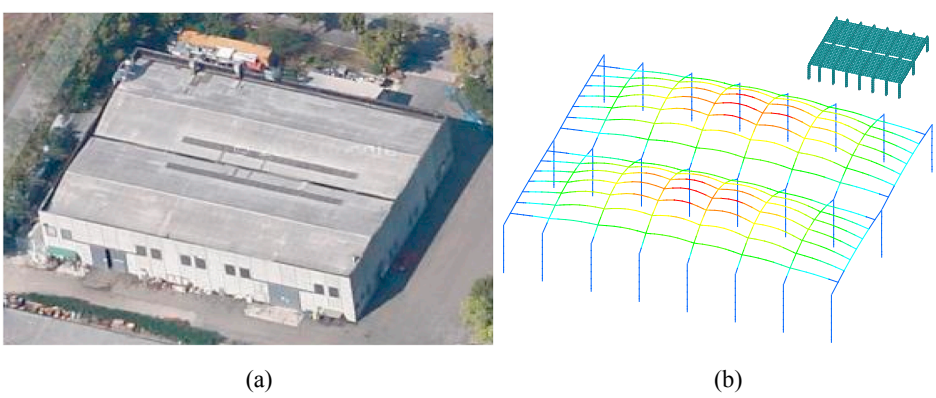

Fig. 14. Case study precast structure considered for validation of the analytical expression for α_{max} proposed in Eq. (2): (a) Aerial view of the building; (b) Deformed shape associated to the first vertical natural period of three-dimensional numerical FE model.

spectral analyses with a behaviour factor $q = 1.5$ as suggested in several building codes for vertical accelerations, shows that the latter systematically underestimates results obtained by time-histories.

This important finding suggests that use of EC8 spectral response analysis could underestimate the vertical force fluctuations induced by earthquakes, resulting in unacceptable safety level estimates. Underestimation can be due to the adoption of $q = 1.5$, because the precast roof elements behave substantially elastically when subject to vertical motion. A revision of the design vertical spectrum should be considered for the class of buildings studied here. The use of the analytical expression proposed in Eq. (2), instead, gives more realistic estimates of the vertical force fluctuations as also confirmed by the case study illustrated in the last section.

It is to highlight that only 3 and 2 ground motions were available for the FF subsets 0.4–0.6g and 0.8–1.0g, respectively. The number of records in the subsets maybe is too small to provide a meaningful statistical elaboration to draw safe conclusions. Nevertheless, the outcomes of the two subsets have been maintained in order to provide a comparison with other subsets.

Near fault excitations with pulse-velocity effects were also

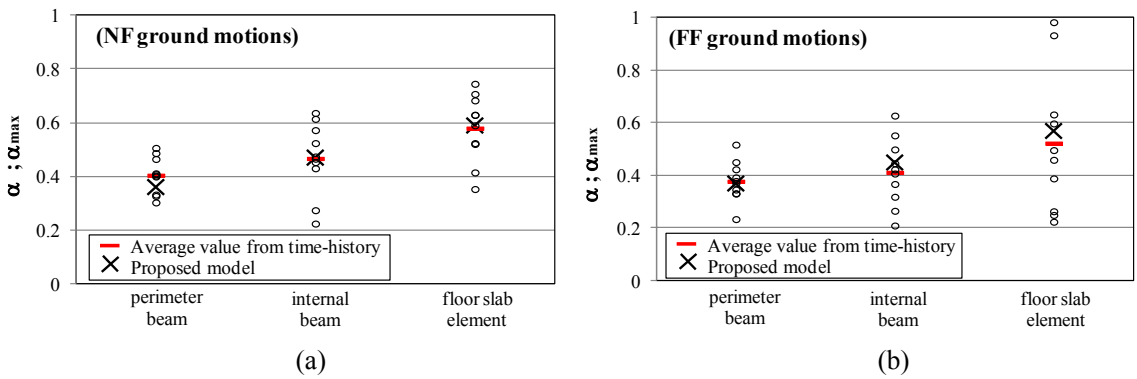

Fig. 15. αmax for the structure depicted in Fig. 14: ○ values obtained via time-history analyses, — average value, × prediction by Eq. (2) for perimeter beams, internal beams and floor slab elements, for $PGA_V = 0.3g$: (a) Near Fault (NF) excitations; (b) Far Fault (FF) excitations.

investigated by means of time-history analyses. From the comparison with the non-pulse-velocity records, a significant increase of the vertical force fluctuations emerged. Further studies to this regard are needed in order to establish a reliable and suitable relation between pulse-velocity shape and vertical force fluctuation increase.

Furthermore, for the class of buildings considered here, the vertical dynamic behaviour at the level of each individual storey was found almost independent from other storeys (when present) and, even more important, the vertical oscillation behaviour is almost independent of the intensity of the horizontal excitation (the latter influencing in a negligible way the vertical dynamic response if the connection capacity is not reached, see Appendix A). These results allow introducing decisive simplification in the numerical modelling for the study of horizontal elements of the examined building class and could be considered in design guidelines or codes.

Lastly, PSA_V was assessed as the best predictors of the seismic vertical force fluctuations expected for this type of buildings, whereas PGA_V and PGV_V are scarcely correlated with α_{max}. This is due to the fact that roof/storey oscillations caused by the vertical component of the earthquake occur almost in the linear range.

Finally, the analytical expression proposed in Eq. (2) is guided by design purposes, where only the PGA_V at the site is required. In fact, the outcomes of this study indicate a poor correlation between the non-dimensional shape of elastic spectrum for vertical acceleration proposed by international codes and the spectrum of recorded vertical ground motions. Hence, if PSA_V, estimated from the codes, was introduced in Eq. (2), significant errors in the evaluation of α_{max} could be expected. For this reason, the authors proposed an analytical expression requiring, in the design phase, only the PGA_V. The β function introduced in Eq. (3) has the role of expressing the dependence on the natural period in a way which is more accurate than adopting the vertical spectrum proposed by codes.

Acknowledgements

The present investigation was developed within the activities of the (Italian) University Network of Seismic Engineering Laboratories – ReLUIS in the research program funded by the (Italian) National Civil Protection – Research Line "Reinforced Concrete Structures 2018", WP2.

Appendix A. Evaluation of the horizontal-vertical interaction

In order to confirm the outcomes announced in Section 4.1 and concerning the horizontal-vertical ground motion interaction, a series of time-history analyses were conducted considering all the three ground motion records of a seismic event (2 horizontal and 1 vertical records). The analyses were conducted considering the three components of 30 different earthquakes, with 10 ground motions selected from each group (i.e., NF, FF and PV). NF and PV subsets records were selected in the range of moment magnitude Mw from 4.0 to 7.9, with a PGA_V ranging from 0.10*g* to 0.7*g*, a distance from causing source between 0 km and 15 km, A, B or C site classes according to EC8, strike-slip, normal, reverse or reverse oblique faults, *PGVv* between 5 cm/s and 70 cm/s and geometric mean PGA_H from 0.10*g* to 2.0*g*. FF subset records were selected in the range of moment magnitude Mw from 4.0 to 7.9, with a PGA_V ranging from 0.10*g* to 0.5*g*, a distance from causing source between 15 km and 50 km, A, B or C site classes according to EC8, strike-slip, normal, reverse or reverse oblique faults, *PGVv* between 3 cm/s and 20 cm/s and geometric mean PGA_H from 0.10*g* to 2.0*g*.

No-scaling procedures were applied to the records, so the components of the selected inputs are those registered during the events. After selection, horizontal components have PGA_H values ranging from 0.10*g* to 1.74*g*, pushing the models widely into nonlinear range.

The main results from the time-history analyses performed on structures S1, S9 and V4 of the building stock in Fig. 3 (first natural vertical period *T* of 0.328 s, 0.185 s and 0.110 s, respectively) are then reported in Fig. A1, in terms of α_{max} for perimeter beams, internal beams and floor slab elements. The vertical seismic component only (1D) or, instead, all three components (vertical + horizontal + horizontal, 3D) were alternatively prescribed for a comparison of results. The figure shows that, for both beams and floor-slab elements, almost all results are located in proximity to the diagonal line, indicating that very close values of α_{max} are obtained by considering 1D and 3D seismic inputs. The maximum difference is 7.2%, 8.5% and 1.4%, respectively, for NF, FF and PV excitations, whereas considering the average values of α_{max} for each group of seismic events (NF, FF and PV) the difference is 1.43%, 0.98% and 1.49%, respectively.

We can then conclude that the horizontal acceleration components influence only in a marginal way the vertical response of horizontal structural elements of the building type considered in the present paper. This is a crucial point because, as a general consequence, the vertical dynamic response of this class of precast buildings can be investigated without performing a full nonlinear time-history analysis with both horizontal and vertical components. This outcome gives considerable advantages connected to the ground motion selection, time-saving in the modelling phase, numerical analyses and post-processing of results.

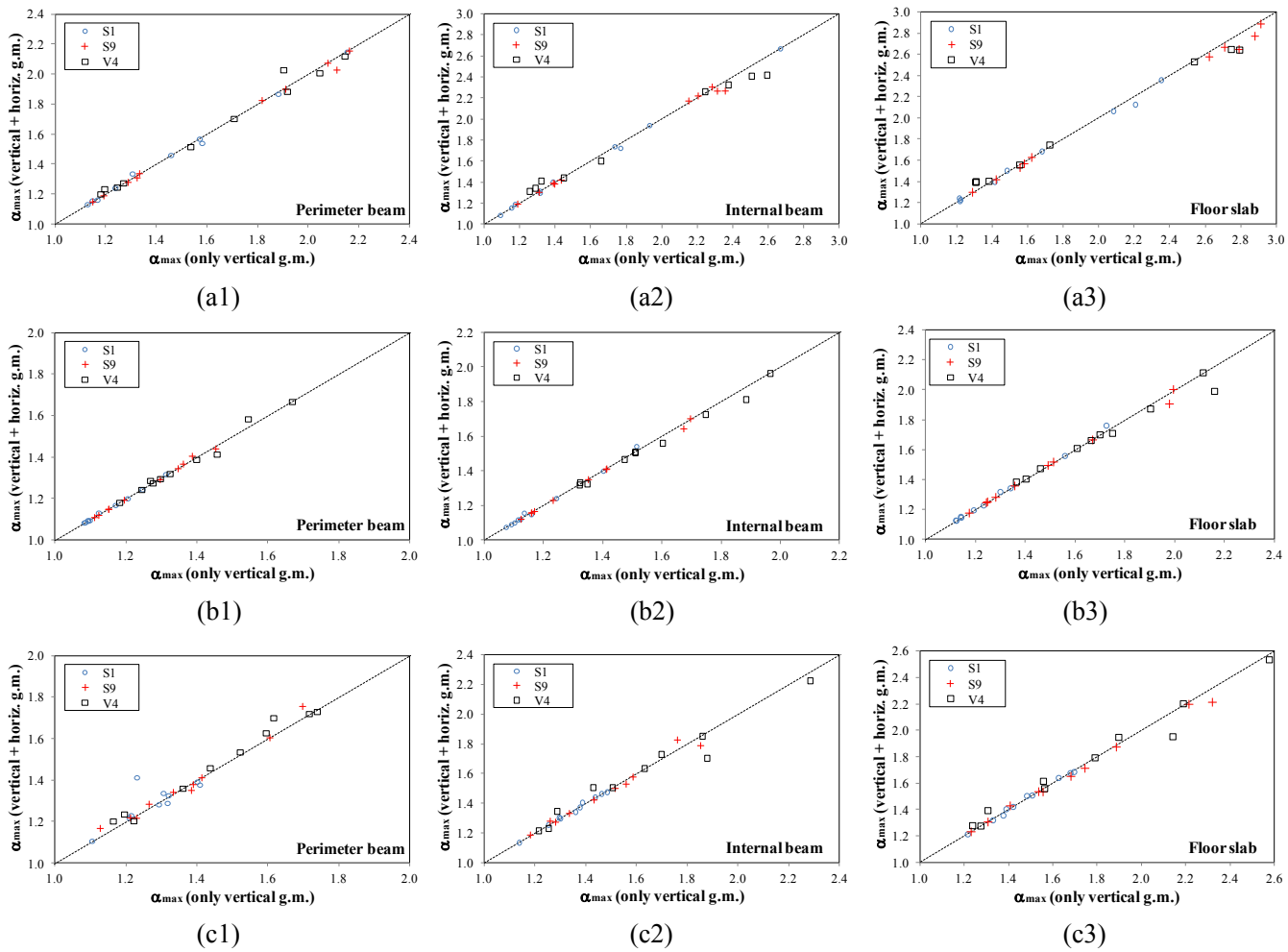

Fig. A1. α_{max} for perimeter beams, internal beams and floor slab elements considering all the three ground motions (g.m.) components of an earthquake vs. α_{max} considering the only vertical ground motion component (for buildings S1, S9 and V4). (a) NF ground motions; (b) FF ground motions; (c) PV ground motions.

Appendix B. Supplementary material

Supplementary data to this article can be found online at https://doi.org/10.1016/j.engstruct.2018.10.018.

References

[1] Papazoglou AJ, Elnashai AS. Analytical and field evidence of the damaging effect of vertical earthquake ground motion. Earthquake Eng Struct Dyn 1996;25:1109–37.
[2] Benedetti D, Carydis P. Influence of the vertical component on damage during shallow near field earthquakes. Eur Earthquake Eng 1999;3:3–12.
[3] Salazar AR, Haldar A. Structural responses considering the vertical component of earthquakes. Comput Struct 2000;74(2):131–45.
[4] Elgamal A, He L. Vertical earthquake ground motion records: an overview. J Earthquake Eng 2004;8(5):663–97.
[5] Ambraseys N, Douglas J. Reappraisal of the effect of the vertical ground motion response. ESEE report N. 4; 2000.
[6] Dana M, Cussen A, Chen YN, Davis C, Greer M, Houston J, Littler P, Roufegarinejad A. Effects of the seismic vertical component on structural behavior – an analytical study of current code practices and potential areas of improvement. Proceedings of the 10th national conference in earthquake engineering, Anchorage, AK. 2014.
[7] FEMA356. Prestandard and commentary for the seismic rehabilitation of buildings. Federal Emergency Management Agency; 2000.
[8] NZS 1170. Structural design actions. Standards New Zealand; 2004.
[9] EC8. Eurocode 8-Part 1: General rules, seismic actions and rules for building. Brussels (Belgium): European Prestandard EN 1998-1; 2005.
[10] NTC. Italian building code. Ministerial Decree 14/01/2008; 2008.
[11] Abrahamson NA, Litehiser JJ. Attenuation of vertical peak acceleration. Bull Seismol Soc Am 1989;79(3):549–80.
[12] Bozorgnia Y, Niazi M. Distance scaling of vertical and horizontal response spectra of the Loma Prieta earthquake. Earthquake Eng Struct Dyn 1993;22:695–707.
[13] Ambraseys NN, Simpson KA. Prediction of vertical response spectra in Europe. Earthquake Eng Struct Dyn 1996;25:401–12.
[14] Campbell KW, Bozorgnia Y. Updated near-source ground motion (attenuation) relations for the horizontal and vertical components of peak ground acceleration and acceleration response spectra. Bull Seismol Soc Am 2003;93(1):314–31.
[15] Kalkan E, Gülkan P. Empirical attenuation equations for vertical ground motion in Turkey. Earthquake Spectra 2004;20(3):853–82.
[16] Aghabarati H, Tehranizadeh M. Prediction of vertical peak ground acceleration and vertical acceleration response spectra from shallow crustal earthquakes. J Appl Sci 2009;9:1153–8.
[17] Bozorgnia Y, Campbell KW. The vertical-to-horizontal response spectral ratio and tentative procedures for developing simplified V/H and vertical design spectra. J Earthquake Eng 2004;8(2):175–207.
[18] Kunnath SK, Erduran E, Chai YH, Yashinsky M. Effect of near-fault vertical ground motions on seismic response of highway overcrossings. J. Bridge Eng 2008;13(3):282–90.
[19] Savoia M, Mazzotti C, Buratti N, Ferracuti B, Bovo M, Ligabue V, et al. Damages and collapses in industrial precast buildings after the Emilia earthquake. Ingegneria Sismica 2012;29(2):120–31.
[20] Magliulo G, Ercolino M, Petrone C, Coppola O, Manfredi G. The Emilia earthquake: seismic performance of precast reinforced concrete buildings. Earthquake Spectra 2014;30(2):891–912.
[21] Bournas DA, Negro P, Taucer F. Performance of industrial buildings during the Emilia earthquakes in Northern Italy and recommendations for their strengthening. Bull Earthquake Eng 2014;12(5):2383–404.
[22] Braga F, Gigliotti R, Monti G, Morelli F, Nuti C, Salvatore W, et al. earthquake. Bull Earthquake Eng 2012;12(5):2405–18.
[23] Minghini F, Ongaretto E, Ligabue V, Savoia M, Tullini N. Observational failure analysis of precast buildings after the 2012 Emilia earthquakes. Earthquake Struct

2016;11(2):327–46. https://doi.org/10.12989/eas.2016.11.2.327.
[24] Savoia M, Buratti N, Vincenzi L. Damage and collapse in industrial precast buildings after the 2012 Emilia earthquake. Eng Struct 2017. [accepted for publication].
[25] Buratti N, Minghini F, Ongaretto E, Savoia M, Tullini N. Empirical seismic fragility for the precast RC industrial buildings damaged by the 2012 Emilia (Italy) earthquakes. Earthquake Eng Struct Dyn 2017;46(14):2317–35.
[26] Iverson JK, Hawkins NM. Performance of precast/prestressed concrete building structures during Northridge Earthquake. PCI J 1994;39(2):38–56.
[27] Posada M, Wood SL. Seismic performance of precast industrial buildings in Turkey. Proceedings of the 7th U.S. National Conference on Earthquake Engineering, Boston. 2002. Paper 543.
[28] Khare RK, Maniyar MM, Uma SR, Bidwai VB. Seismic performance and design of precast concrete building structures: an overview. J Struct Eng 2011;38(3):272–84.
[29] Senel SM, Palanci M. Structural aspects and seismic performance of 1-story precast buildings in Turkey. J Perform Constr Facil 2013;27(4):437–49.
[30] Tapan M, Comert M, Demir C, Sayan Y, Orakcal K, Ilki A. Failures of structures during the October 23, 2011 Tabanlı (Van) and November 9, 2011 Edremit (Van) earthquakes in Turkey. Eng Fail Anal 2013;34:606–28. https://doi.org/10.1016/j.engfailanal.2013.02.013.
[31] Ozden S, Akpinar E, Erdogan H, Atalay H. Performance of precast concrete structures in October 2011 Van earthquake, Turkey. Mag Concr Res 2014;66(11):543–52. https://doi.org/10.1680/macr.13.00097.
[32] Carydis P, Castiglioni C, Lekkas E, Kostaki I, Lebesis N, Drei A. The Emilia Romagna, May 2012 earthquake sequence. The influence of the vertical earthquake component and related geoscientific and engineering aspects. Ingegneria Sismica 2012;29(2–3):31–58.
[33] Liberatore L, Sorrentino L, Liberatore D, Decanini LD. Failure of industrial structures induced by the Emilia (Italy) 2012 earthquakes. Eng Fail Anal 2013;34:629–47.
[34] Belleri A, Brunesi E, Nascimbene R, Pagani M, Riva P. Seismic performance of precast industrial facilities following major earthquakes in the Italian territory. J Perform Constr Facil 2014;29(5):04014135.
[35] Bovo M, Savoia M. Numerical Simulation of seismic-induced failure of a precast structure during the Emilia earthquake. J Perform Constr Facil 2018;32(1):04017119.
[36] Park R, Priestley MJN, Gill WD. Ductility of square-confined concrete columns. ASCE J Struct Div 1982;108(4):929–50.
[37] Ghobarah A, Elnashai AS. Contribution of vertical ground motion to the damage of R/C buildings. Proceedings of the 11th European Conference on Earthquake Engineering, Balkema, Rotterdam. 1988.
[38] Bhide SB, Collins MP. Influence of axial tension on the shear capacity of reinforced concrete members. ACI Struct J 1989;86(5):570–81.
[39] Kim SJ, Elnashai AS. Characterization of shaking intensity distribution and seismic assessment of RC buildings for the Kashmir (Pakistan) earthquake of October 2005. Eng Struct 2009;31:2998–3015.
[40] Makan KD, Chen Y, Larkin T, Chouw N. The influence of vertical seismic ground motion on structures with uplift. New Zealand society for earthquake engineering conference. 2013.
[41] Diotallevi PP, Landi L. Effect of the axial force and of the vertical ground motion component on the seismic response of R/C frames. Proceedings of the 12th world conference on earthquake engineering, Upper Hutt, New Zealand. 2000. Paper No. 1026.
[42] Carydis P. The vertical seismic component "The Columbus egg in earthquake Engineering. 12th European conference on earthquake engineering, London. 2002. Paper 868.
[43] Mwafy AM. Effect of bidirectional excitations on seismic response of RC buildings. J Earthquake Tsunami 2012;6(3). https://doi.org/10.1142/S1793431112500194.
[44] Magliulo G, Fabbrocino G, Manfredi G. Seismic assessment of existing precast industrial buildings using static and dynamic nonlinear analyses. Eng Struct 2008;30:2580–8.
[45] Casotto C, Silva V, Crowley H, Nascimbene R, Pinho R. Seismic fragility of Italian RC precast industrial structures. Eng Struct 2015;94:122–36.
[46] Bolognini D, Borzi B, Pinho R. Simplified pushover-based vulnerability analysis of traditional Italian RC precast structures. Proceedings of the 14th world conference on earthquake engineering, Beijing, China. 2008.
[47] Brunesi E, Nascimbene R, Bolognini D, Bellotti D. Experimental investigation of the cyclic response of reinforced precast concrete framed structures. PCI J 2015;60(2):57–79.
[48] Bournas DA, Negro P, Molina FJ. Pseudodynamic tests on a full-scale 3-storey precast concrete building: behavior of the mechanical connections and floor diaphragms. Eng Struct 2013;57:609–27.
[49] Magliulo G, Ercolino M, Cimmino M, Capozzi V, Manfredi G. Cyclic shear test on a dowel beam-to-column connection of precast buildings. Earthquake Struct 2015;9(3):541–62.
[50] Psycharis IN, Mouzakis HP. Shear resistance of pinned connections of precast members to monotonic and cyclic loading. Eng Struct 2012;41:413–27.
[51] PEER. Ground motion database. Pacific Earthquake Engineering Research Center; 2010 [accessed 10 January 2015].
[52] PEER. Final report of the NGA-West2 directivity working group. PEER report 2013/09; 2013.
[53] Chopra AK, Chintanapakdee C. Comparing response of SDF systems to near-fault and far-fault earthquake motions in the context of spectral regions. Earthquake Eng Struct Dyn 2001;30:1769–89. https://doi.org/10.1002/eqe.92.
[54] Martinez-Pereira A, Bommer JJ. What is the near-field? Seismic Design Practice into the Next Century. Rotterdam: Booth Editions; 1998. p. 245–52.
[55] Mavroeidis GP, Dong G, Papageorgiou AS. Near-fault ground motions, and the response of elastic and inelastic single-degree-of-freedom (SDOF) systems. Earthquake Eng Struct Dyn 2004;33:1023–49. https://doi.org/10.1002/eqe.391.
[56] Somerville PG. Engineering characterization of near fault ground motions. New Zealand society for earthquake engineering conference. 2005.
[57] Maniatakis CA, Taflampas IM, Spyrakos CC. Identification of near-fault earthquake record characteristics. Proceedings of 14th world conference on earthquake engineering, Beijing, China. 2008.
[58] Mimoglou P, Ioannis N, Psycharis IN, Taflampas IM. Explicit determination of the pulse inherent in pulse-like ground motions. Earthquake Eng Struct Dyn 2014;43:2261–81. https://doi.org/10.1002/eqe.2446.
[59] Kardoutsou V, Mimoglou P, Taflampas IM, Psycharis IN. Evaluation and comparison of new methods for the classification of ground motions as pulse-like or non pulse-like. Proceedings of SECED conference. Cambridge (UK). 2015.
[60] Mander JB, Priestley MJN, Park R. Theoretical stress-strain model for confined concrete. ASCE J Struct Eng 1988;114(8):1804–26.
[61] Menegotto M, Pinto PE. Method of analysis for cyclically loaded R.C. plane frames including changes in geometry and non-elastic behavior of element under combined normal force and bending. Proceedings IABSE symp of resistance and ultimate deformability of structures acted on by well-defined repeated loads. Lisbon (Portugal): International Association of Bridge and Structural Engineering; 1973.
[62] EC2. Eurocode 2-Part 1: General rules and rules for buildings. Brussels (Belgium): European Prestandard EN 1992-1-1; 2004.
[63] STYL v1.0; 2015. http://www.reluis.it [accessed 10 January 2015].
[64] Spacone E, Filippou FC, Taucer FF. Fibre beam-column model for non-linear analysis of R/C frames: part I Formulation. Earthquake Eng Struct Dyn 1996;25:711–25.
[65] OpenSEES v2.4.0. Open system for earthquake engineering simulation. Pacific Earthquake Engineering Research Center; 2015.
[66] Collier CJ, Elnashai AS. A procedure for combining vertical and horizontal seismic action effects. J Earthquake Eng 2001;5(4):521–39.
[67] Bradley BA, Cubrinovski M. Near-source strong ground motions observed in the 22 February 2011 Christchurch Earthquake. Bull N Zeal Soc Earthquake Eng 2011;44(4):181–94.
[68] Iervolino I, De Luca F, Chioccarelli E. Engineering seismic demand in the 2012 Emilia sequence: preliminary analysis and model compatibility assessment. Ann Geophys 2012;55(4). https://doi.org/10.4401/ag-6118.
[69] Akkar S, Özen Ö. Effects of peak ground velocity on deformation demands for SDOF systems. Earthquake Eng Struct Dyn 2005;34(13):1551–71.
[70] Malhotra PK. Response of buildings to near-field pulse-like ground motions. Earthquake Eng Struct Dyn 1999;28:1309–26.
[71] Spyrakos CC, Maniatakis CA, Taflambas J. Evaluation of near source seismic records based on damage potential parameters. Case study: Greece. Soil Dyn Earthquake Eng 2008;28:738–53.
[72] Hayden CP, Bray JD, Abrahamson NA. Selection of near-fault pulse motions. J Geotech Geoenviron Eng 2014;140:04014030.